Fat and water separation techniques in NMR imaging

Noura Azzabou
30 April 2013

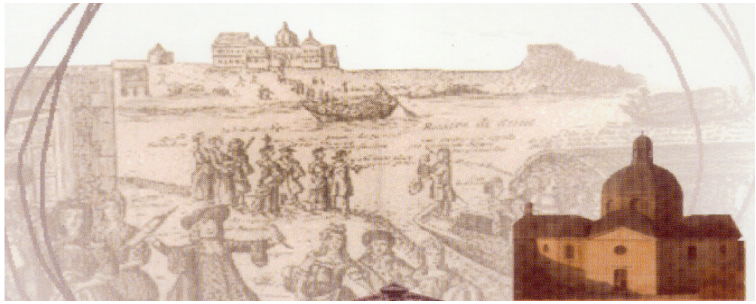


Fat and water separation techniques : chemical shift principle

A vector representation of the complex signal S for a a given pixel with two spectral components, water (W) and fat (F).

$$S(TE) = \left(\mathrm{W} + \mathrm{F}\ \mathrm{e}^{\mathrm{i}2\pi\Delta\mathrm{f}\ \mathrm{TE}}\right)\mathrm{e}^{\mathrm{i}2\pi\Delta\mathrm{B}_0\mathrm{TE}}\mathrm{e}^{\theta_0}$$

The phase angle of fat relative to that of water due to their chemical shift difference

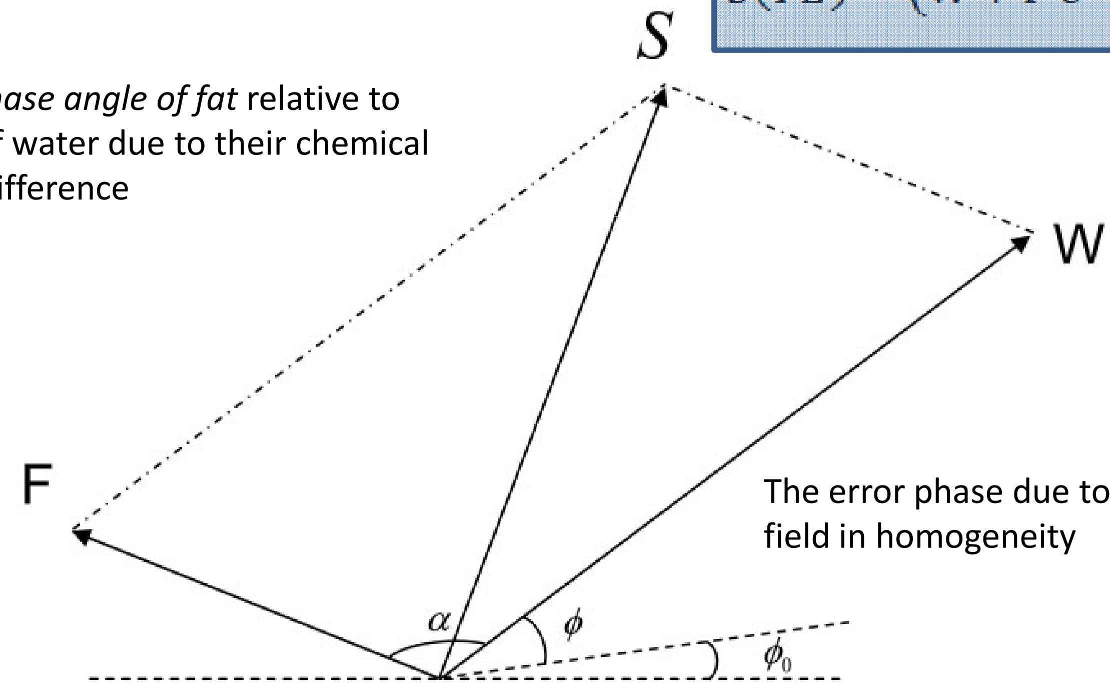

The error phase due to the magnetic field in homogeneity

another error phase due to other system imperfections such as the spatial dependence of RF penetration and different signal delay in the receiver chains.

Fat and water separation techniques : chemical shift principle

A vector representation of the complex signal S for a a given pixel with two spectral components, water (W) and fat (F).

$$S(TE) = \left(W + F\, e^{i2\pi\Delta f\, TE}\right) e^{i2\pi\Delta B_0 TE} e^{\theta_0}$$

The phase angle of fat relative to that of water due to their chemical shift difference

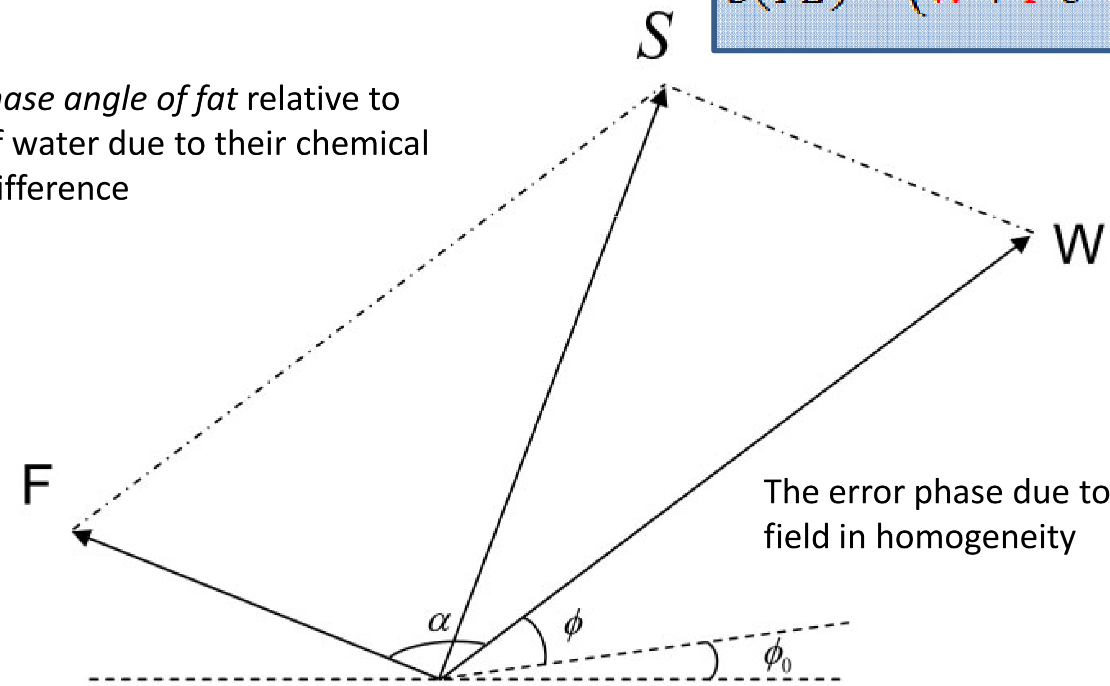

The error phase due to the magnetic field in homogeneity

another error phase due to other system imperfections such as the spatial dependence of RF penetration and different signal delay in the receiver chains.

Fat and water separation techniques : 2 point Dixon

Acquisition : Echos time selection

Assuming that water-fat chemical shift (σ) is 3.5 ppm, and B_0 = 3T

3.5 ppm @ 3T = $\sigma B_0 \gamma$ = 3.5 x 3 x 42.58 MHz/T= 447 Hz

relative phase = $2\pi\Delta f\,TE$ = TE x 447 x 2π

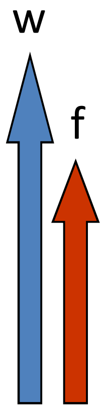

("in phase" condition)

TEi= 1/447 s = 2.24 ms

TEi= 2/447 s = 4.48 ms

$$S(TE_i) = (W + F)e^{i2\pi\Delta B_0 TE_i}e^{\theta_0}$$

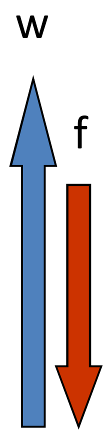

("opposed phase" condition)

TEo= 1.5/447 s = 3.36 ms

TEo= 3/447 s = 6.71 ms

$$S(TE_o) = S_o = (W - F)e^{i2\pi\Delta B_0 TE_o}e^{\theta_0}$$

Fat and water separation techniques : 2 point Dixon

Water and Fat signal reconsutruction

$$S(TE_i) = S_i = (W + F)e^{i2\pi\Delta B_0 TE_i}e^{\theta_0}$$
$$S(TE_o) = S_o = (W - F)e^{i2\pi\Delta B_0 TE_o}e^{\theta_0}$$

$$\rightarrow$$

$$|S_i| = |W + F|$$
$$|S_o| = |W - F|$$

Assuming a prior knowledge about fat water content and that for example there is more fat than water in the pixel we can write

$$W = \frac{|S_i| + |S_o|}{2} \qquad F = \frac{|S_i| - |S_o|}{2}$$

In the opposite case we have

$$F = \frac{|S_i| + |S_o|}{2} \qquad W = \frac{|S_i| - |S_o|}{2}$$

Fat and water separation techniques : 2 point Dixon

Reconstruction results

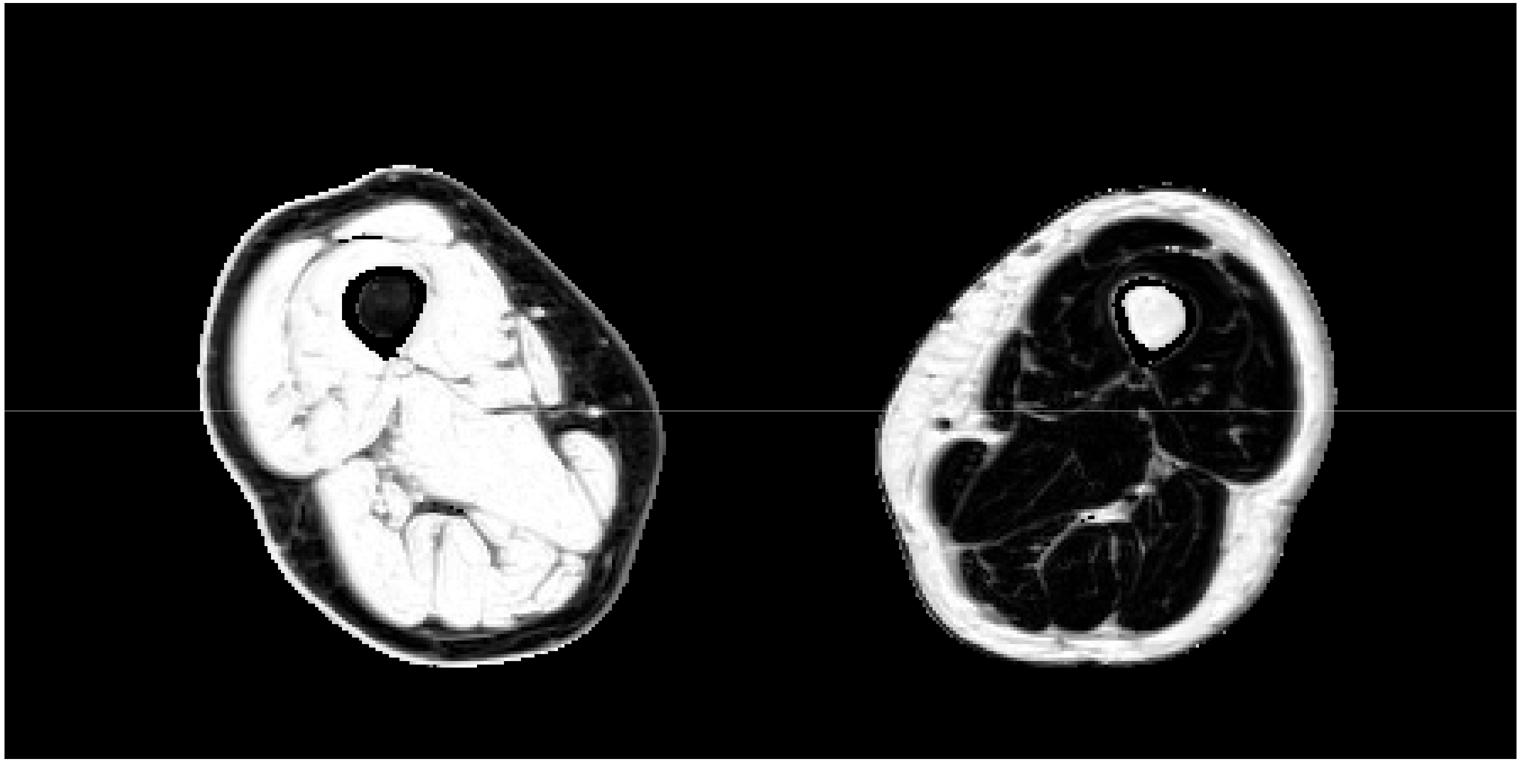

Fat ratio map, for the thigh of healthy volunteer.

Fat and water separation techniques : 2 point Dixon

Reconstruction results

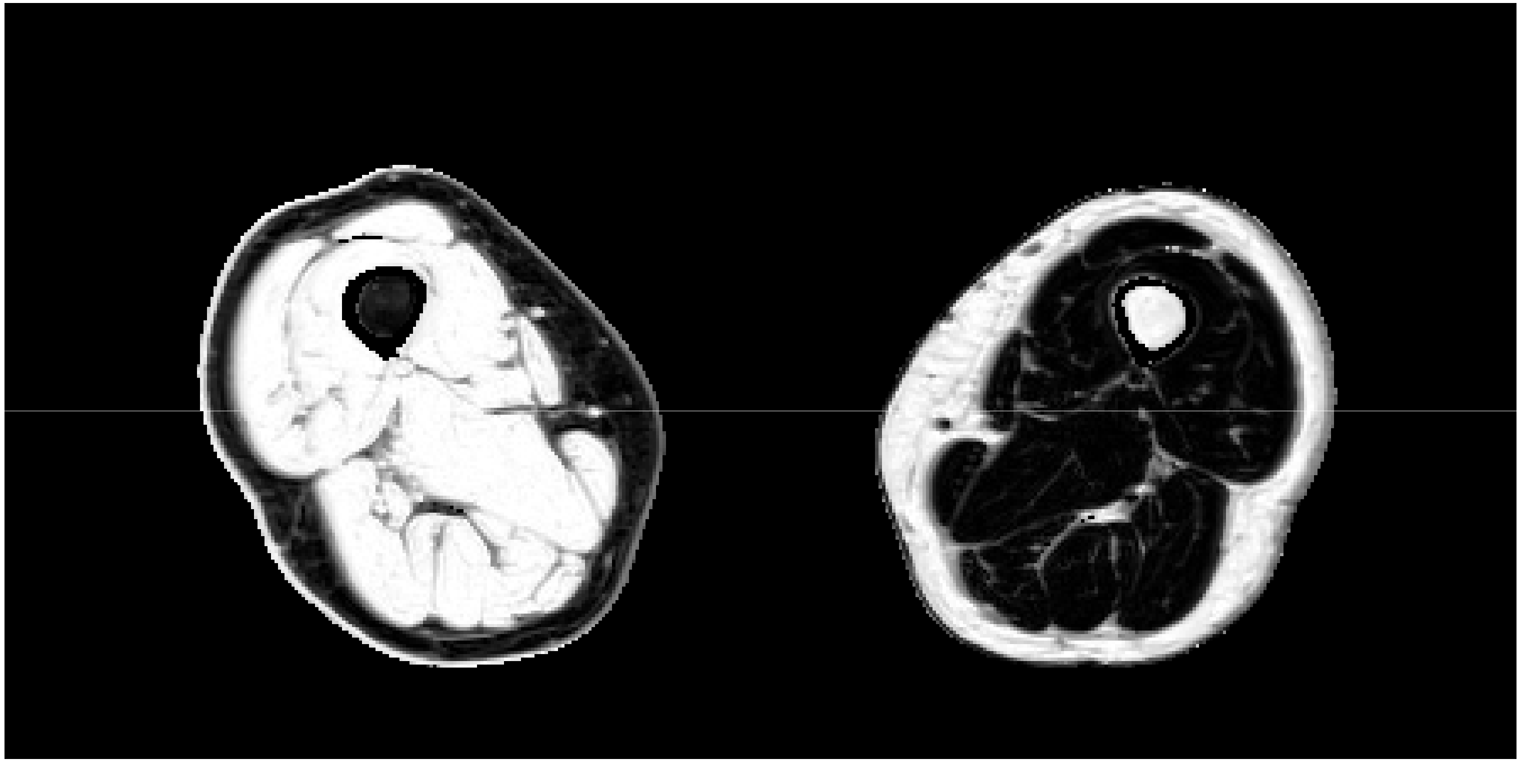

Fat ratio map, for the thigh of healthy volunteer. For the one leg water and fat signal are swapped

Fat and water separation techniques : 3 point Dixon

Reconstruction technique

$$S(TE_1) = S_1 = (W + F)e^{i2\pi\Delta B_0 TE_1} e^{\theta_0}$$

$$S(TE_2) = S_2 = (W - F)e^{i2\pi\Delta B_0 TE_2} e^{\theta_0}$$

$$S(TE_1) = S_3 = (W + F)e^{i2\pi\Delta B_0 TE_3} e^{\theta_0}$$

$$\mathrm{Arg}(S_3) - \mathrm{Arg}(S_1) = 2\pi\Delta B_0(TE_3 - TE_1) + 2k\pi$$

After computing B0 inhomogenieties, fat and water signal are computed through linear equation resolving.

Fat and water separation techniques : 3 point Dixon

Phase wrapping problem

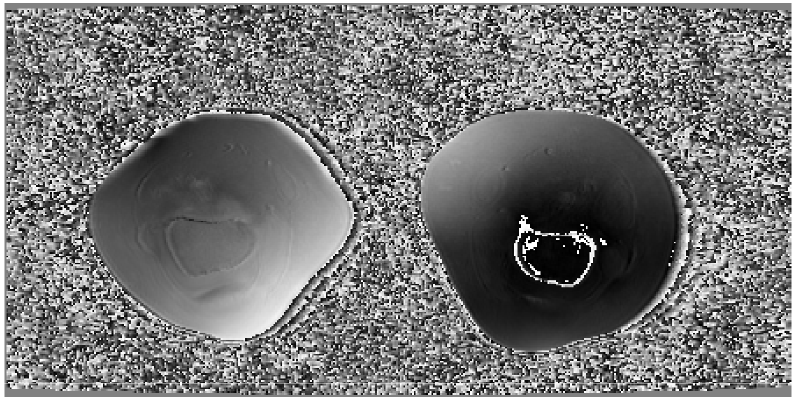

Phase of the first in-phase image S1

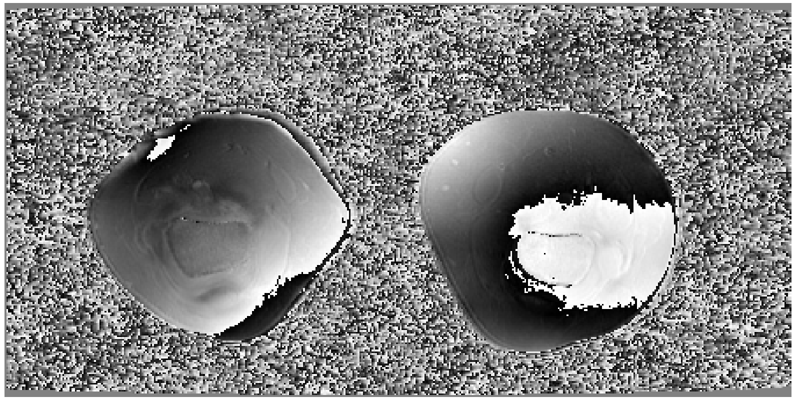

Phase of the second in-phase image S3

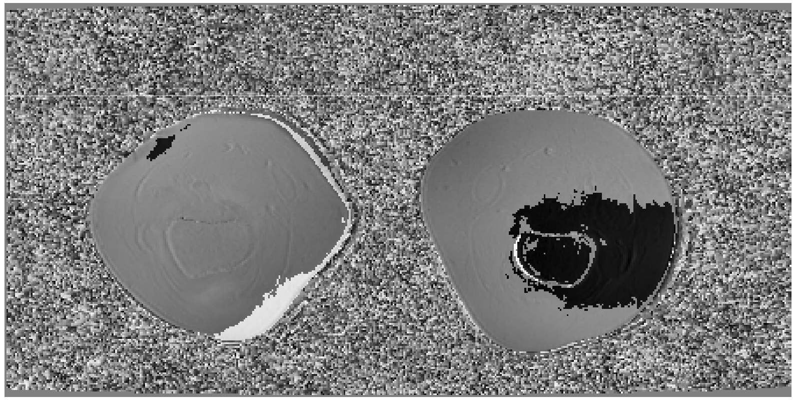

Difference between phases.

Fat and water separation techniques : 3 point Dixon

Phase wrapping problem

Fast and robust three-dimensional best path phase unwrapping algorithm

Hussein S. Abdul-Rahman,[1] Munther A. Gdeisat,[1,*] David R. Burton,[1] Michael J. Lalor,[1] Francis Lilley,[1] and Christopher J. Moore[2]

[1]General Engineering Research Institute (GERI), Liverpool John Moores University, James Parsons Building Room 114, Byrom Street, Liverpool L3 3AF, UK

[2]North West Medical Physics, Developing Technologies Section, Christie Hospital NHS Foundation Trust, Wilmslow Road, Manchester M20 4BX, UK

*Corresponding author: m.a.gdeisat@ljmu.ac.uk

Fat and water separation techniques : 3 point Dixon

Phase wrapping problem

The proposed algorithm can be summarized in the following steps:

1. Determine the qualities of all voxels.
2. Calculate the horizontal, vertical, and normal edges's qualities and set the qualities of the edges that are connected with the borders to zero in order to be processed last.
3. Sort all of the edges according to their qualities in descending order.
4. Unwrap voxels according to the edges qualities, so that the voxels that form the highest quality edges are unwrapped first according to the following rules:
   A. If both voxels do not belong to any group and have not been unwrapped before, the voxels are unwrapped with respect to each other and gathered into a single group.
   B. If one of the voxels has been processed before and belongs to a group, but the other has not, then the voxel that has not been processed before is unwrapped with respect to the other voxels in the group and now joins this group.
   C. If both voxels have been processed before and both belong to different groups, then the two groups are unwrapped with respect to each other. The smaller group is unwrapped with respect to the larger group. Then the two groups are joined together to construct a single group.

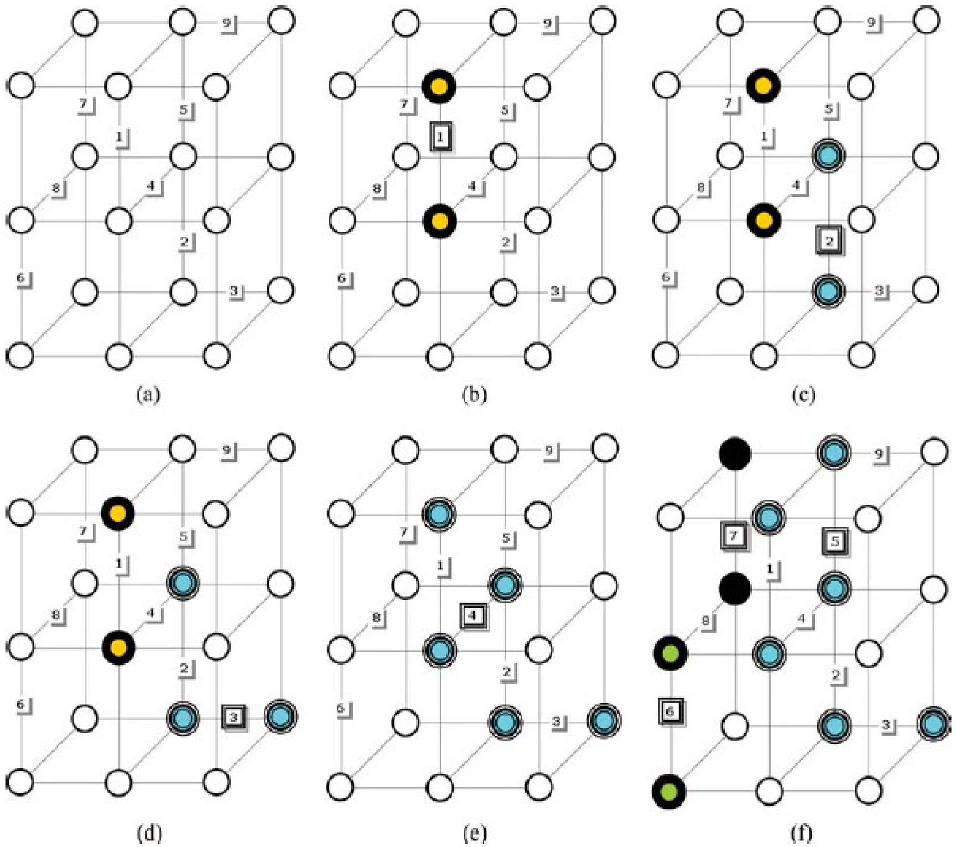

Fig. 2. (Color online) Demonstration of the unwrapping path of the proposed algorithm.

Fat and water separation techniques : 3 point Dixon

Example of reconstructed images

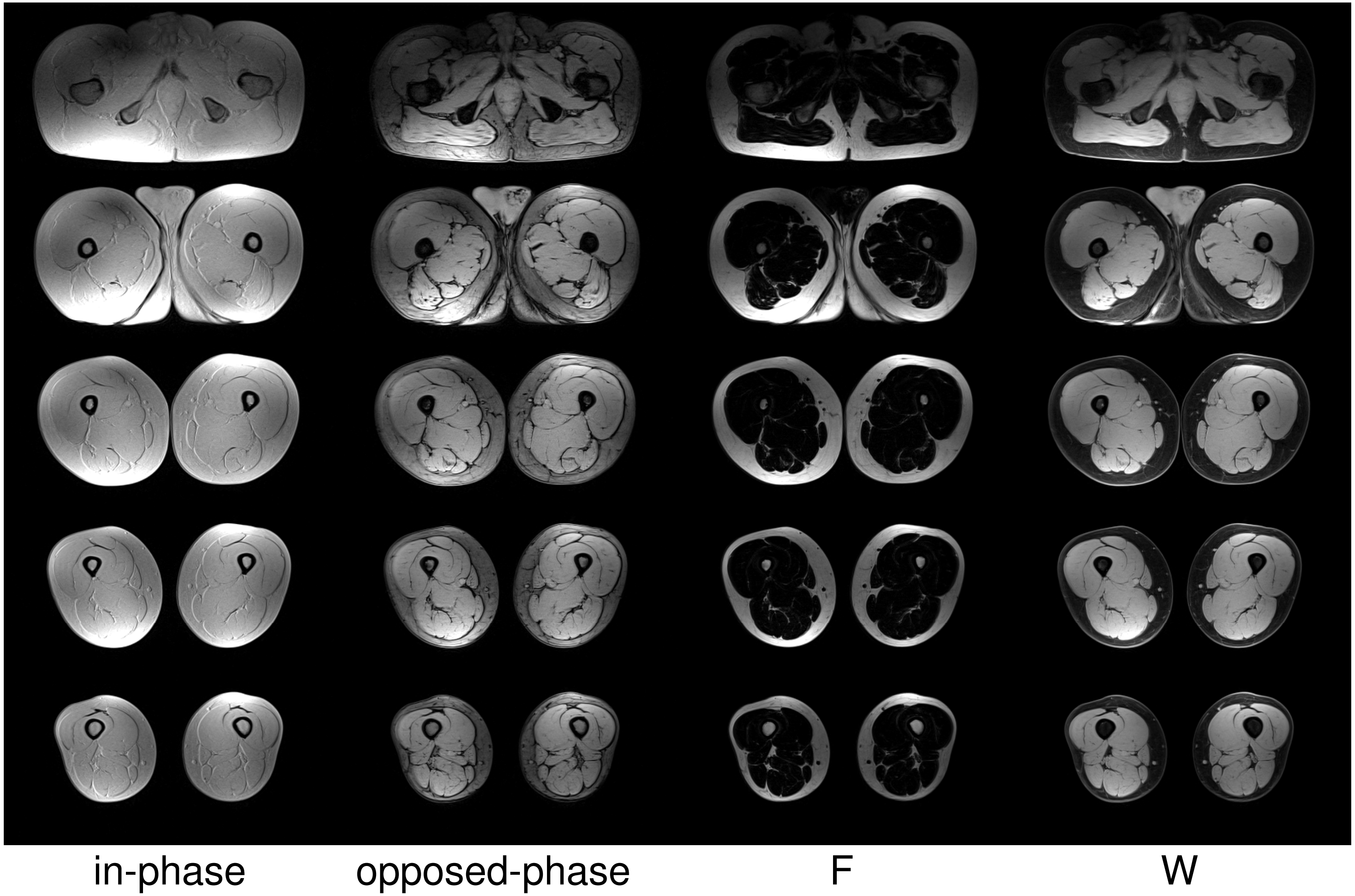

Fat and water separation techniques : 3 point Dixon

Quantitative analysis

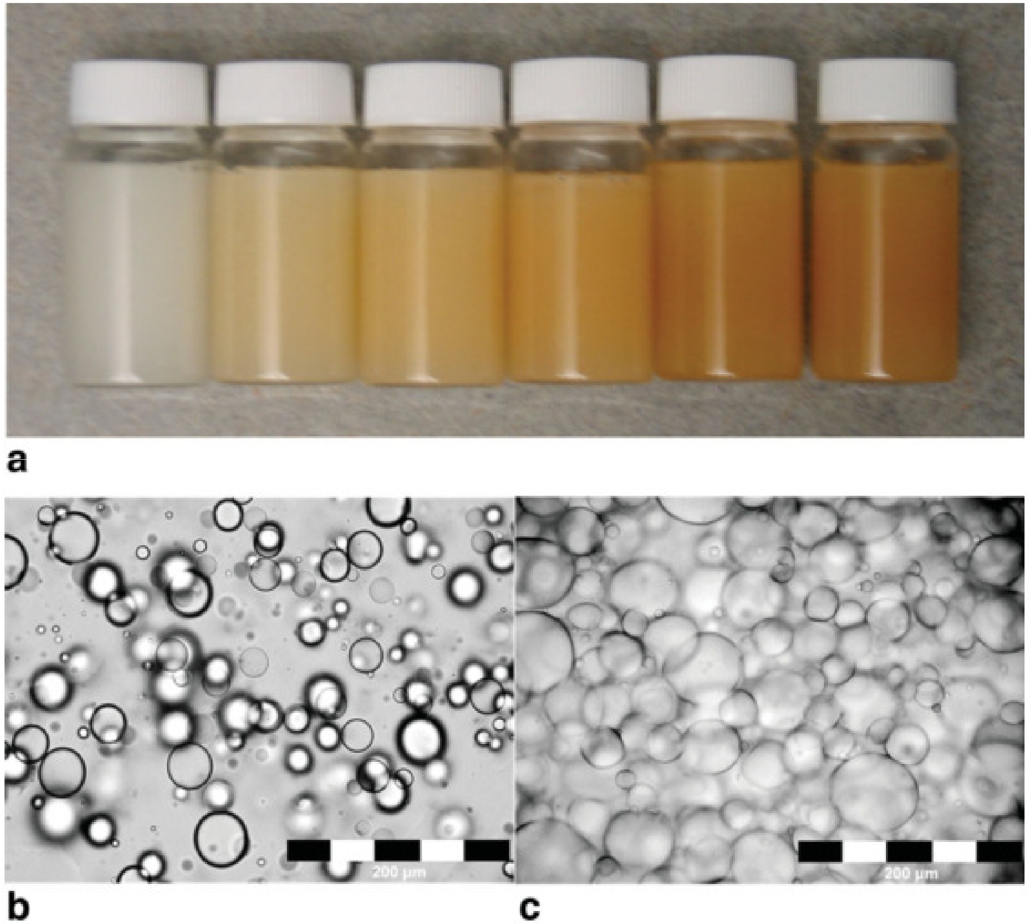

Figure 1. a: Photograph of vials containing 20% fat with iron concentrations of 0, 10, 20, 30, 40, and 50 μg Fe/mL (left to right) demonstrate successful homogenization of fat, water, and iron components. Vials are lying horizontally to demonstrate that the resulting product, with the exception of 100% peanut oil, is a rigid gel at room temperature. Photomicrographs (20×) of 50% fat (**b**) and 10% fat (**c**) emulsions with 20 μg Fe/mL. Lipid globules are easily visible as round structures, and are confirmed not to be air bubbles by a surgical pathologist. Although the vials are macroscopically homogeneous, lipid globules are easily visible and create microscopic heterogeneity. The mean diameter of the globules in the 50% fat emulsion is 234 ± 66 μm, and 47 ± 19 μm for the 10% fat emulsion.

Reference : Hines, C. D. G., Yu, H., Shimakawa, A., McKenzie, C. a, Brittain, J. H., & Reeder, S. B. (2009). T1 independent, T2* corrected MRI with accurate spectral modeling for quantification of fat: validation in a fat-water-SPIO phantom. *Journal of magnetic resonance imaging: JMRI*, *30*(5), 1215-22.

Fat and water separation techniques : 3 point Dixon

Quantitative analysis

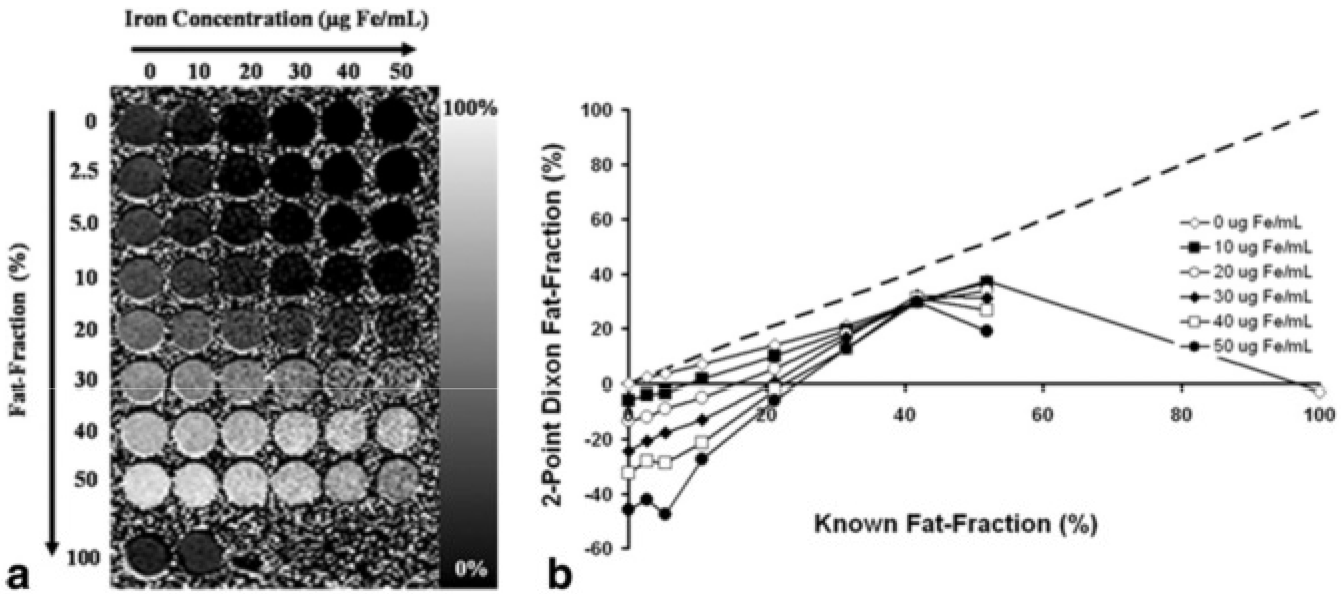

Figure 3. Fat-fractions measured using conventional 2-point Dixon imaging. **a:** The fat-fraction image calculated using Equation 2 shows decreasing apparent fat-fraction (%) with increasing iron concentration (µg Fe/mL). **b:** Measurements from regions of interest from this image are also plotted. The ambiguity known to occur with fat-fractions more than 50% is demonstrated with the 100% fat vial, which has an apparent fat-fraction close to 0.0 (−2.98 ± 0.25%). Linear regression results show excellent correlation ($r^2 = 0.99$) for fat-fractions at 0 µg Fe/mL when the 100% vial is omitted. Slope = 0.72 ± 0.01 ($P << 0.001$), intercept = −0.48 ± 0.40% ($P = 0.26$), although the slope indicates underestimation of fat-fraction. Dashed line represents unity.

Reference : Hines, C. D. G., Yu, H., Shimakawa, A., McKenzie, C. a, Brittain, J. H., & Reeder, S. B. (2009). T1 independent, T2* corrected MRI with accurate spectral modeling for quantification of fat: validation in a fat-water-SPIO phantom. *Journal of magnetic resonance imaging: JMRI*, *30*(5), 1215-22.

Fat and water separation techniques : 3 point Dixon

Quantitative analysis

Table 1
Two-Point Dixon Fat-Fractions and Chemical Shift-Based Fat-Fractions Compared to Known Fat-Fractions

	0 μg Fe/mL	10 μg Fe/mL	20 μg Fe/mL	30 μg Fe/mL	40 μg Fe/mL	50 μg Fe/mL
Conventional two-point Dixon						
R^{2a}	0.99	0.99	0.99	0.97	0.96	0.91
Slope[a]	0.72 ± 0.01	0.84 ± 0.02	0.97 ± 0.04	1.18 ± 0.08	1.32 ± 0.11	1.54 ± 0.20
	$P << 0.001$	$P << 0.001$	$P = 0.5$	$P = 0.05$	$P = 0.03$	$P = 0.03$
Intercept[a]	−0.0048 ± 0.0039	−0.068 ± 0.0051	−0.14 ± 0.010	−0.23 ± 0.021	−0.32 ± 0.03	−0.45 ± 0.053
	$P = 0.26$	$P << 0.001$	$P << 0.001$	$P << 0.001$	$P << 0.001$	$P = 0.00006$
Single-peak reconstruction without T_2^a correction						
R^2	0.96	0.98	0.99	0.97	0.99	0.99
Slope	0.94 ± 0.07	0.81 ± 0.05	1.00 ±0.05	1.12 ± 0.03	1.1 ± 0.04	1.17 ± 0.05
	$P = 0.5$	$P = 0.01$	$P = 0.94$	$P = 0.01$	$P = 0.01$	$P = 0.02$
Intercept	−0.034 ± 0.030	0.021 ± 0.013	0.023 ± 0.013	0.043 ± 0.0085	0.054 ± 0.012	0.075 ± 0.014
	$P = 0.3$	$P = 0.2$	$P = 0.07$	$P = 0.001$	$P = 0.003$	$P = 0.001$
Multipeak reconstruction without T_2^a correction						
R^2	0.99	0.99	0.99	0.99	0.98	0.97
Slope	0.93 ± 0.02	0.96 ± 0.03	1.06 ± 0.02	1.08 ± 0.04	1.07 ± 0.06	1.00 ± 0.07
	$P = 0.01$	$P = 0.2$	$P = 0.05$	$P = 0.1$	$P = 0.3$	$P = 0.9$
Intercept	0.044 ± 0.0089	0.10 ± 0.0075	0.15 ± 0.00066	0.21 ± 0.010	0.25 ± 0.015	0.30 ± 0.020

Reference : Hines, C. D. G., Yu, H., Shimakawa, A., McKenzie, C. a, Brittain, J. H., & Reeder, S. B. (2009). T1 independent, T2* corrected MRI with accurate spectral modeling for quantification of fat: validation in a fat-water-SPIO phantom. *Journal of magnetic resonance imaging: JMRI*, *30*(5), 1215-22.

Fat and water separation techniques : 3 point Dixon

Quantitative analysis

Dixon technique is based on the chemical shift difference between water protons and lipid –CH2 protons.

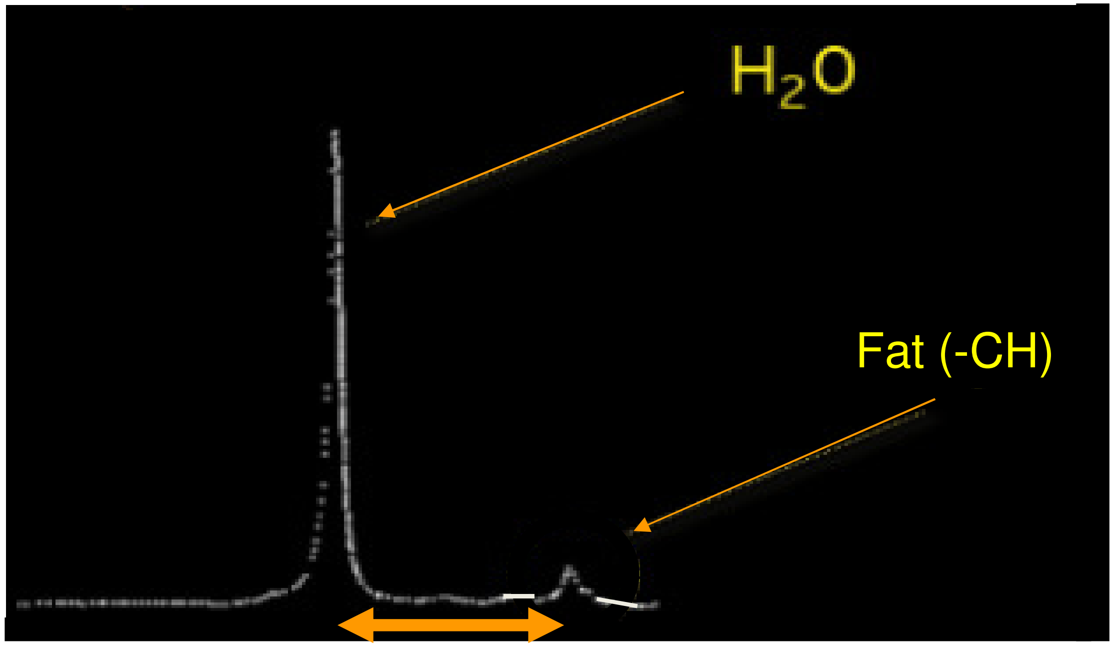

~3.5 ppm ~ 450 Hz @ 3T

Fat and water separation techniques : Fat spectrum

Peak	Chemical Shift	Triacylglycerol-Associated [1]H of the Spectra
P_1	0.90 ppm	$C\underline{H}_3-(CH_2)_n-$
P_2	1.30 ppm	$-(C\underline{H}_2)_n-$
P_3	1.60 ppm	$-CH_2-O-CO-CH_2-C\underline{H}_2-$
P_4	2.03 ppm	$-CH_2-C\underline{H}_2-CH=CH-$
P_5	2.25 ppm	$-CH_2-O-CO\ -C\underline{H}_2-CH_2-$
P_6	2.76 ppm	$-CH=CH-C\underline{H}_2-CH=CH-$
P_7	4.09 ppm	$-C\underline{H}_2-O-C(O)-CH_2-CH_2-$
P_8	4.28 ppm	-C[illegible]-C(O)-CH_2-CH_2-
P_9	5.32 ppm	-C[illegible]- and >C$\underline{H}$-CH_2-O-C(O)-CH_2-CH_2-

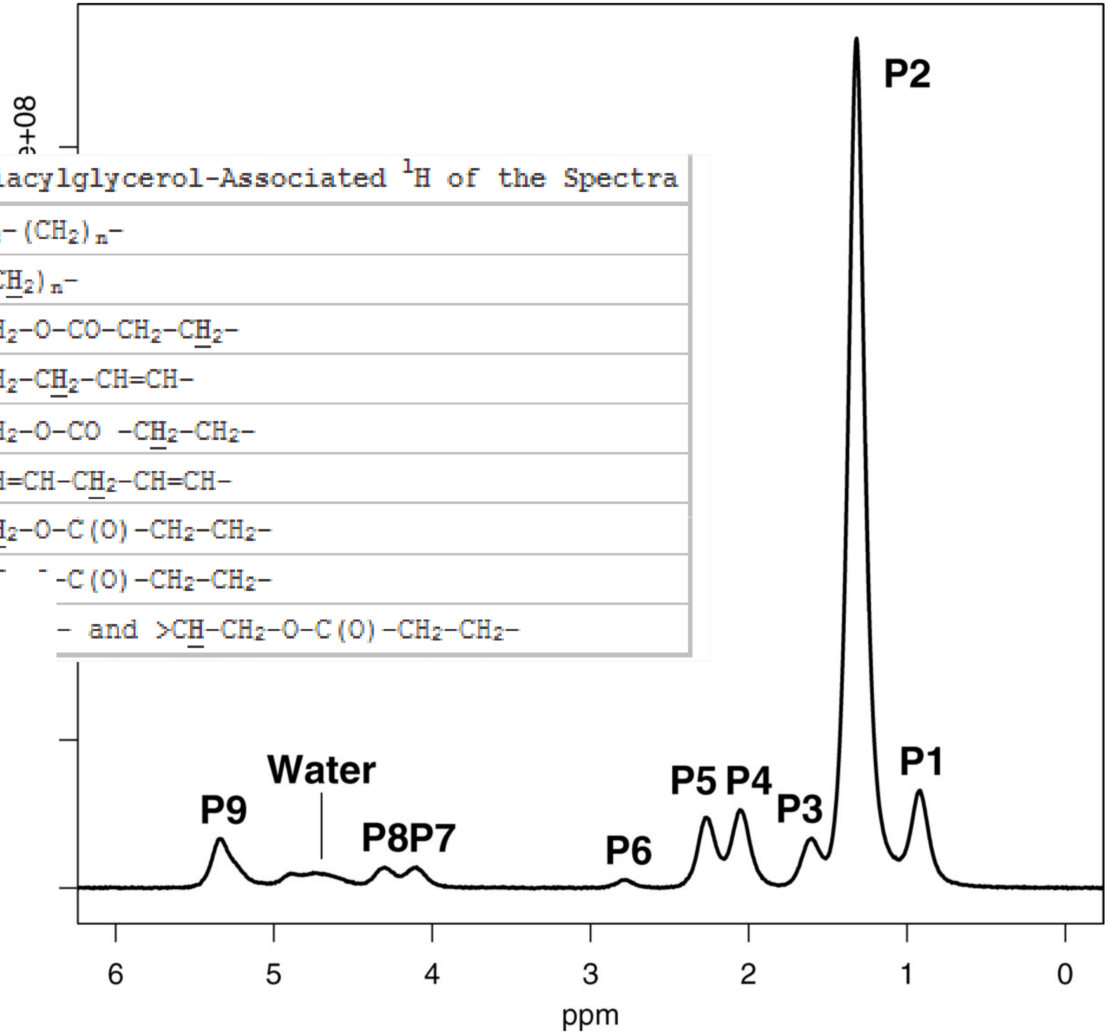

Strobel K et al. J. Lipid Res. 2008;49:473-480

Representative localized in vivo proton spectrum (PRESS: TR = 1.8 s, TE = 20 ms, voxel size = 2 mm × 2 mm × 2 mm, NEX = 500) of adipose tissue of a mouse.

Fat and water separation techniques : Multi-peak Model

Signal Model

Consider the signal in an image from a pixel containing M species, each with chemical shift (Hz), Δf_j ($j = 1, \ldots, M$) located at position $\mathbf{r}$, acquired at a TE, t,

$$s(t) = \left(\sum_{j=1}^{M} \rho_j e^{i2\pi\Delta f_j t} \right) e^{i2\pi\psi t} \qquad [1]$$

where ρ_j is the intensity of the jth species and is, in general, a complex term with its own magnitude, $|\rho_j|$, and phase, ϕ_j, and ψ is the local magnetic resonance offset (Hz). If measurements are made at discrete echo times, t_n ($n = 1, \ldots, N$), then,

$$s_n = \left(\sum_{j=1}^{M} \rho_j e^{i2\pi\Delta f_j t_n} \right) e^{i2\pi\psi t_n} \qquad [2]$$

Fat and water separation techniques : Multi-peak Model

Signal Model

Consider the signal in an image from a pixel containing M species, each with chemical shift (Hz), Δf_j ($j = 1, \ldots, M$) located at position $\mathbf{r}$, acquired at a TE, t,

$$s(t) = \left(\sum_{j=1}^{M} \rho_j e^{i2\pi \Delta f_j t} \right) e^{i2\pi \psi t} \qquad [1]$$

where ρ_j is the intensity of the jth species and is, in general, a complex term with its own magnitude, $|\rho_j|$, and phase, ϕ_j, and ψ is the local magnetic resonance offset (Hz). If measurements are made at discrete echo times, t_n ($n = 1, \ldots, N$), then,

$$s_n = \left(\sum_{j=1}^{M} \rho_j e^{i2\pi \Delta f_j t_n} \right) e^{i2\pi \psi t_n} \qquad [2]$$

Magnetic Resonance in Medicine 51:35–45 (2004

Multicoil Dixon Chemical Species Separation With an Iterative Least-Squares Estimation Method

Scott B. Reeder,* Zhifei Wen, Huanzhou Yu, Angel R. Pineda, Garry E. Gold, Michael Markl, and Norbert J. Pelc

IDEAL - ALGORITHM

$$s_n = \left(w + \sum_{k=1}^{M} \rho_k \, e^{i2\pi\Delta f_k t_n}\right) e^{i2\pi\psi t_n}$$

We can formulate this as a linear system with respect to fat and water signal.

$$\begin{pmatrix} s_1 \\ s_2 \\ \\ \\ s_N \end{pmatrix} = A * \begin{pmatrix} w \\ \rho_1 \\ \rho_2 \\ \\ \rho_M \end{pmatrix} \qquad A = \begin{pmatrix} e^{i2\pi\psi t_1} & e^{i2\pi\psi t_1} e^{i2\pi\Delta f_k t_1} \\ e^{i2\pi\psi t_2} & e^{i2\pi\psi t_1} e^{i2\pi\Delta f_k t_2} \\ \\ \\ e^{i2\pi\psi t_N} & e^{i2\pi\psi t_1} e^{i2\pi\Delta f_k t_N} \end{pmatrix}$$

In order to resolve this system we have to acquire at least M+2 images (with M total number of fat peaks).

Magnetic Resonance in Medicine 51:35–45 (2004

Multicoil Dixon Chemical Species Separation With an Iterative Least-Squares Estimation Method

Scott B. Reeder,* Zhifei Wen, Huanzhou Yu, Angel R. Pineda, Garry E. Gold, Michael Markl, and Norbert J. Pelc

IDEAL - ALGORITHM $s_n = \left(w + \sum_{k=1}^{M} \rho_k \, e^{i2\pi\Delta f_k t_n}\right) e^{i2\pi\psi t_n}$

If we assume that $\psi = \psi_0$ is known than finding w and ρ_k amounts to a linear system resolving

$$A = \begin{pmatrix} e^{i2\pi\psi_0 t_1} & e^{i2\pi\psi_0 t_1} e^{i2\pi\Delta f_k t_1} \\ e^{i2\pi\psi_0 t_2} & e^{i2\pi\psi_0 t_1} e^{i2\pi\Delta f_k t_2} \\ & \\ & \\ e^{i2\pi\psi_0 t_N} & e^{i2\pi\psi_0 t_1} e^{i2\pi\Delta f_k t_N} \end{pmatrix} \quad \Longrightarrow \quad \begin{pmatrix} w \\ \rho_1 \\ \rho_2 \\ \\ \rho_M \end{pmatrix} = [conj(A) * A]^{-1} conj(A) \begin{pmatrix} s_1 \\ s_2 \\ \\ \\ s_N \end{pmatrix}$$

Fat and water separation techniques : IDEAL technique

Iterative reconstruction process

Using the above equations and those in the appendices, the following algorithm summarizes the method used to determine the least-squares estimates of water images and fat images for each pixel:

1. Estimate the signal from each chemical species using Eq. [A3] and an initial guess for the field map, ψ_o. A useful initial guess for ψ_o is zero (Hz).
2. Calculate the error to the field map, $\Delta\psi$, using Eq. [B7].
3. Recalculate $\psi = \psi_o + \Delta\psi$.
4. Recalculate $\hat{s}_n$ (Eqs. [3] and [4]) with the new estimate of ψ.
5. Repeat the preceding three steps until $\Delta\psi$ is small (e.g., $<$1 Hz).
6. Spatially filter (smooth) the final field map, ψ, with a low-pass filter.
7. Recalculate the final estimate of each chemical species image with Eq. [A3].

The final field map is filtered to improve noise performance, as discussed below.

Fat and water separation techniques : IDEAL technique

Iterative reconstruction process : field map error estimation

If $\rho_j^R = \hat{\rho}_j^R + \Delta\rho_j^R$ and $\rho_j^I = \hat{\rho}_j^I + \Delta\rho_j^I$ $(j = 1, \ldots, M)$, and $\psi = \psi_o + \Delta\psi$, then Eq. [2] can be written as

$$s_n \approx \left(\sum_{j=1}^{M} (\hat{\rho}_j + \Delta\rho_j) e^{i2\pi\Delta f_j t_n} \right) e^{i2\pi\psi_o t_n} e^{i2\pi\Delta\psi t_n}. \qquad [B1]$$

Dividing each side by $e^{i2\pi\psi_o t_n}$, and using the Taylor approximation $e^{i2\pi\Delta\psi t_n} \approx 1 + i2\pi\Delta\psi t_n$, such that

$$\hat{s}_n^R + i\hat{s}_n^I = \left(\sum_{j=1}^{M} (\hat{\rho}_j^R + \Delta\rho_j^R + i(\hat{\rho}_j^I + \Delta\rho_j^I))(c_{jn} + id_{jn}) \right) \times (1 + i2\pi\Delta\psi t_n). \qquad [B2]$$

Fat and water separation techniques : IDEAL technique

Iterative reconstruction process : field map error estimation

Rearranging Eq. [B2], and splitting into real

$$\hat{s}_n^R = s_n^R - \sum_{j=1}^{M} (\hat{\rho}_j^R c_{jn} - \hat{\rho}_j^I d_{jn}) = 2\pi\Delta\psi t_n \sum_{j=1}^{M} (-\hat{\rho}_j^R d_{jn} - \hat{\rho}_j^I c_{jn}) + \sum_{j=1}^{M} \Delta\rho_j^R c_{jn} - \sum_{j=1}^{M} \Delta\rho_j^I d_{jn} \quad [B3]$$

and imaginary components

$$\hat{s}_n^I = s_n^I - \sum_{j=1}^{M} (\hat{\rho}_j^R d_{jn} + \hat{\rho}_j^I c_{jn}) = 2\pi\Delta\psi t_n \sum_{j=1}^{M} (\hat{\rho}_j^R c_{jn} - \hat{\rho}_j^I d_{jn}) + \sum_{j=1}^{M} (\Delta\rho_j^R d_{jn} + \Delta\rho_j^I c_{jn}) \quad [B4]$$

where $\hat{s}_n^R$ and $\hat{s}_n^I$ are defined in Eqs. [B3] and [B4]. Arranging in matrix format for $n = 1, \ldots, N$:

$$\hat{\mathbf{S}} \approx \mathbf{B}\mathbf{y} \quad [B5]$$

$$\mathbf{y} = [\ \Delta\psi \quad \Delta\rho_1^R \quad \Delta\rho_1^I \quad \Delta\rho_2^R \quad \Delta\rho_2^I \quad \cdots \quad \Delta\rho_M^R \quad \Delta\rho_M^I\ ]^T,$$

$$g_{jn}^R = 2\pi t_n \sum_{j=1}^{M} (-\hat{\rho}_j^R d_{jn} - \hat{\rho}_j^I c_{jn})$$

and $g_{jn}^I = 2\pi t_n \sum_{j=1}^{M} (\hat{\rho}_j^R c_{jn} - \hat{\rho}_j^I d_{jn})$, such that,

$$\mathbf{B} = \begin{bmatrix} g_{11}^R & c_{11} & -d_{11} & c_{21} & -d_{21} & \cdots & c_{M1} & -d_{M1} \\ g_{12}^R & c_{12} & -d_{12} & c_{22} & -d_{22} & \cdots & c_{M2} & -d_{M2} \\ \cdots & \cdots & \cdots & \cdots & \cdots & \cdots & \cdots & \cdots \\ g_{1N}^R & c_{1N} & -d_{1N} & c_{2N} & -d_{2N} & \cdots & c_{MN} & -d_{MN} \\ g_{11}^I & d_{11} & c_{11} & d_{21} & c_{21} & \cdots & d_{M1} & c_{M1} \\ g_{12}^I & d_{12} & c_{12} & d_{22} & c_{22} & \cdots & d_{M2} & c_{M2} \\ \cdots & \cdots & \cdots & \cdots & \cdots & \cdots & \cdots & \cdots \\ g_{1N}^I & d_{1N} & c_{1N} & d_{2N} & c_{2N} & \cdots & d_{MN} & c_{MN} \end{bmatrix}. \quad [B6]$$

For $n = 1, \ldots, N$, Eq. [B5] is also a linear system of equations, and estimates of $\mathbf{y}$ can be calculated (29) by

$$\mathbf{y} = (\mathbf{B}^T\mathbf{B})^{-1}\mathbf{B}^T\hat{\mathbf{S}} \quad [B7]$$

which is used to determine $\Delta\psi$, $\Delta\rho_j^R$, and $\Delta\rho_j^I$.

Fat and water separation techniques : IDEAL technique

Signal Decay

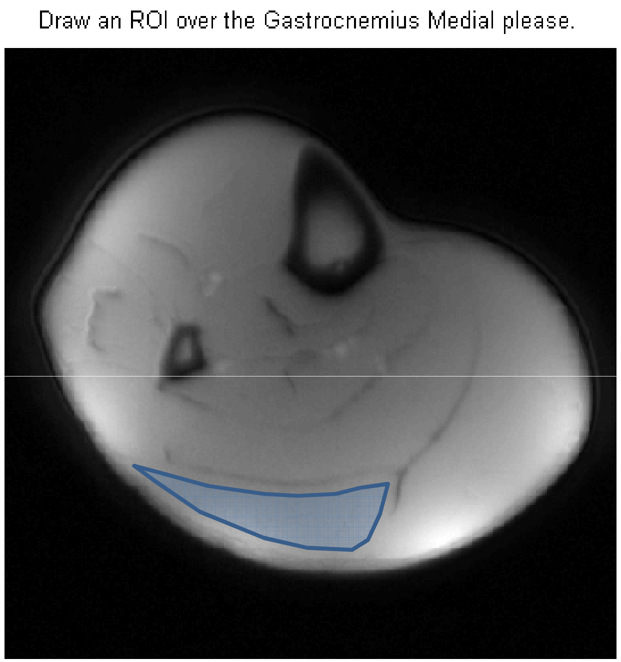

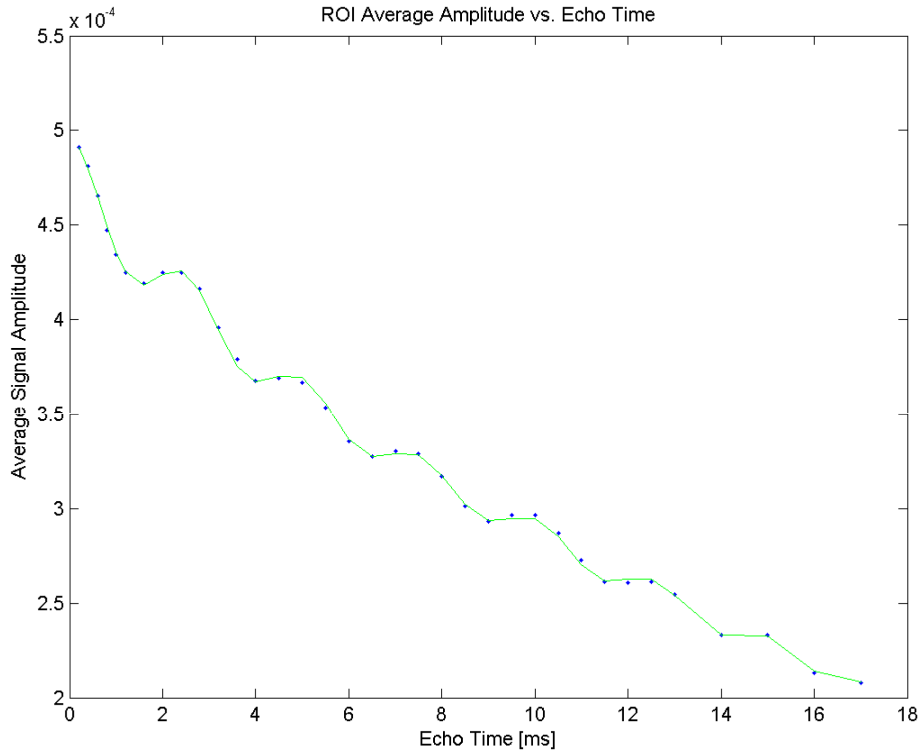

The decay is due to the spin-spin relaxation (T2) and an additional component due to B0 inhomogeniey. The over all decay is called T2* (R2*=1/T2*)

Fat and water separation techniques : IDEAL technique

Signal Decay

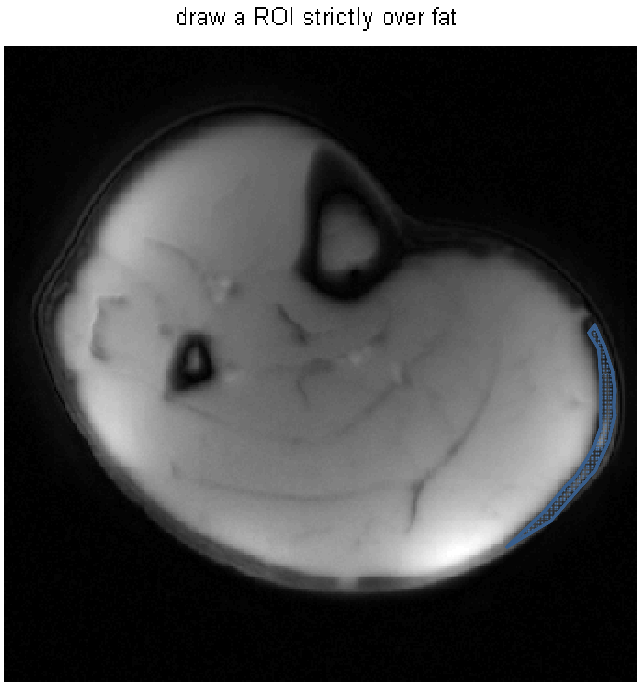

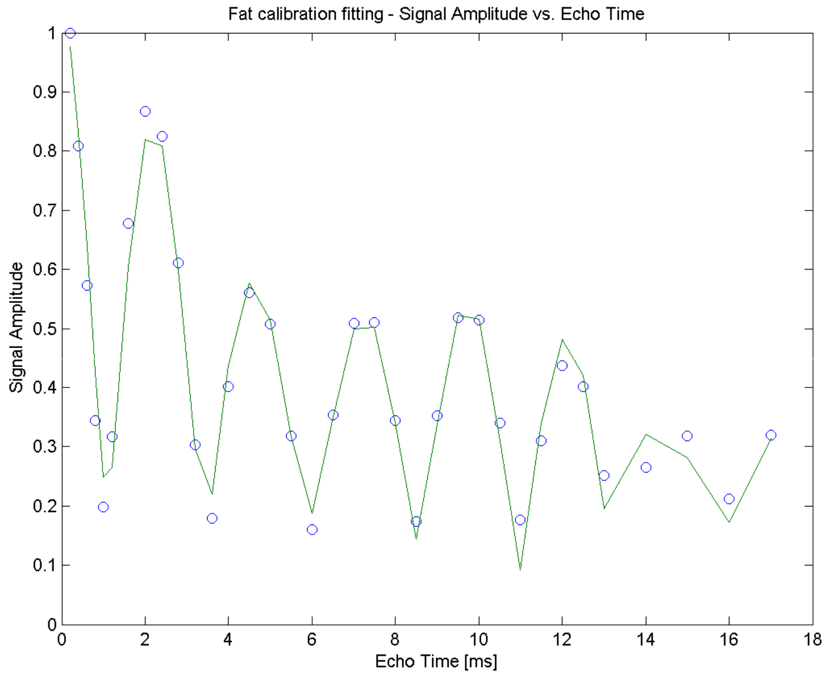

The decay is due to the spin-spin relaxation (T2) and an additional component due to B0 inhomogeniey. The over all decay is called T2* (R2*=1/T2*)

JOURNAL OF MAGNETIC RESONANCE IMAGING 26:1153–1161 (2007)

Technical Note

Multiecho Reconstruction for Simultaneous Water-Fat Decomposition and T2* Estimation

Huanzhou Yu, PhD,[1*] Charles A. McKenzie, PhD,[2] Ann Shimakawa, MS,[1]
Anthony T. Vu, PhD,[3] Anja C.S. Brau, PhD,[1] Philip J. Beatty, PhD,[1]
Angel R. Pineda, PhD,[4] Jean H. Brittain, PhD,[5] and Scott B. Reeder, MD, PhD[6]

$$s_n = \left(w + \sum_{k=1}^{M} \rho_k \, e^{i2\pi\Delta f_k t_n} \right) e^{i2\pi\psi t_n} e^{-t_n R_2^*}$$

If we assume that $\psi = \psi_0$ is known as well as R_2^* than finding w and ρ_k amounts to a linear system resolving

$$A = \begin{pmatrix} e^{i2\pi\psi_0 t_1} e^{-t_1 R_2^*} & e^{i2\pi\psi_0 t_1} e^{i2\pi\Delta f_k t_1} e^{-t_1 R_2^*} \\ e^{i2\pi\psi_0 t_2} e^{-t_2 R_2^*} & e^{i2\pi\psi_0 t_1} e^{i2\pi\Delta f_k t_2} e^{-t_2 R_2^*} \\ & \\ e^{i2\pi\psi_0 t_N} e^{-t_N R_2^*} & e^{i2\pi\psi_0 t_1} e^{i2\pi\Delta f_k t_N} e^{-t_N R_2^*} \end{pmatrix} \Rightarrow \begin{pmatrix} w \\ \rho_1 \\ \rho_2 \\ \\ \rho_M \end{pmatrix} = [conj(A) * A]^{-1} conj(A) \begin{pmatrix} S_1 \\ S_2 \\ \\ S_N \end{pmatrix}$$

Fat and water separation techniques : IDEAL technique

Signal Model with R2* decrease

$$A = D.\begin{pmatrix} 1 & e^{i2\pi\Delta f_k t_1} \\ 1 & e^{i2\pi\Delta f_k t_2} \\ 1 & \\ & \\ 1 & e^{i2\pi\Delta f_k t_N} \end{pmatrix}$$

$$D = diag\left[e^{i2\pi t_1(\psi_0 + iR_2^*)}, e^{i2\pi t_2(\psi_0 + iR_2^*)}, \dots, e^{i2\pi t_N(\psi_0 + iR_2^*)}\right]$$

$$\tilde{\psi} = \psi + iR_2^*$$

The same iterative algorithm is applied with the difference that the unknow field map is a complex number.

Fat and water separation techniques : IDEAL technique

APPENDIX

Modified IDEAL Algorithm to Calculate the Complex Field Map $\hat{\psi}$

With the signals collected at all echoes, Eq. (1) can be formatted in a matrix form:

$$\mathbf{s} = \begin{bmatrix} s_1 \\ s_2 \\ \cdots \\ s_k \end{bmatrix}$$

$$= \begin{bmatrix} e^{j2\pi\hat{\psi}t_1} & 0 & \cdots & 0 \\ 0 & e^{j2\pi\hat{\psi}t_2} & \cdots & 0 \\ \cdots & \cdots & \cdots & \cdots \\ 0 & 0 & \cdots & e^{j2\pi\hat{\psi}t_k} \end{bmatrix} \cdot \begin{bmatrix} 1 & e^{j2\pi\Delta f t_1} \\ 1 & e^{j2\pi\Delta f t_2} \\ \cdots & \\ 1 & e^{j2\pi\Delta f t_k} \end{bmatrix} \cdot \begin{bmatrix} w \\ f \end{bmatrix}$$

$$= \mathrm{P}(\hat{\psi}) \cdot \mathrm{A} \cdot \rho \qquad \text{(A. 1)}$$

$$\mathrm{P}(\hat{\psi}) = \begin{bmatrix} e^{j2\pi\hat{\psi}t_1} & 0 & \cdots & 0 \\ 0 & e^{j2\pi\hat{\psi}t_2} & \cdots & 0 \\ \cdots & \cdots & \cdots & \cdots \\ 0 & 0 & \cdots & e^{j2\pi\hat{\psi}t_k} \end{bmatrix}_{k\times k}$$

$$\mathrm{A} = \begin{bmatrix} 1 & e^{j2\pi\Delta f t_1} \\ 1 & e^{j2\pi\Delta f t_2} \\ \cdots & \\ 1 & e^{j2\pi\Delta f t_k} \end{bmatrix}_{k\times 2}, \quad \rho = \begin{bmatrix} w \\ f \end{bmatrix}_{2\times 1}$$

The vector **s** denotes the acquired signals. The matrix **A** is considered known. The matrix $\mathbf{P}(\hat{\psi})$ is a function of the complex field map and represents the field map and R2* modulation on the signals. The noise term in Eq. (1) has been dropped for convenience. At each pixel the following algorithm is used to estimate the complex field map $\hat{\psi}$.

Fat and water separation techniques : IDEAL technique

1. Starting from the initial guess of the complex field map $\tilde{\hat{\psi}} = \psi_0$. An initial guess of 0 is used for R2* at all pixels. $\tilde{\hat{\psi}}$ represents the current estimate of the "complex field map."
2. With the estimated $\tilde{\hat{\psi}}$, the corresponding complex water $\tilde{\mathrm{w}}$ and fat $\tilde{\mathrm{f}}$ can be determined from a least-squares inversion:

$$\tilde{\rho} = \begin{bmatrix} \tilde{\mathrm{w}} \\ \tilde{\mathrm{f}} \end{bmatrix} = (A^T A)^{-1} A^T \cdot P(-\tilde{\hat{\psi}}) \cdot \mathbf{s} \qquad \text{(A.2)}$$

where $\mathbf{A^T}$ represents the complex conjugate transpose of the $\mathbf{A}$ matrix. Here, we have used the fact that $\mathbf{P}(-\hat{\psi}) \cdot \mathbf{P}(\hat{\psi}) = \mathbf{P}(\hat{\psi}) \cdot \mathbf{P}(-\hat{\psi}) = \mathbf{I}$.

3. Equation (1) can be approximated by Taylor expansion as in the following, with the second and higher-order terms neglected.

$$s_i = (\tilde{\mathrm{w}} + \tilde{\mathrm{f}} \cdot e^{j2\pi\Delta f t_i}) \cdot e^{j2\pi\tilde{\hat{\psi}} t_i} + e^{j2\pi\tilde{\hat{\psi}} t_i} \cdot \Delta\mathrm{w} + e^{j2\pi\tilde{\hat{\psi}} t_i} \cdot e^{j2\pi\Delta f t_i} \Delta\mathrm{f} + (\tilde{\mathrm{w}} + \tilde{\mathrm{f}} \cdot e^{j2\pi\Delta f t_i}) \cdot e^{j2\pi\tilde{\hat{\psi}} t_i} \cdot j2\pi t_i \cdot \Delta\hat{\psi} \qquad \text{(A.3)}$$

Considering all echoes, Eq. (A.3) can be formulated in a matrix form:

$$\mathbf{s} = \mathbf{P}(\tilde{\hat{\psi}}) \cdot \mathbf{A} \cdot \tilde{\rho} + \mathbf{P}(\tilde{\hat{\psi}}) \cdot \begin{bmatrix} (\tilde{\mathrm{w}} + \tilde{\mathrm{f}} \cdot e^{j2\pi\Delta f t_1}) \cdot j2\pi t_1 & 1 & e^{j2\pi\Delta f t_1} \\ (\tilde{\mathrm{w}} + \tilde{\mathrm{f}} \cdot e^{j2\pi\Delta t_2}) \cdot j2\pi t_2 & 1 & e^{j2\pi\Delta f t_2} \\ \cdots & \cdots & \cdots \\ (\tilde{\mathrm{w}} + \tilde{\mathrm{f}} \cdot e^{j2\pi\Delta t_k}) \cdot j2\pi t_k & 1 & e^{j2\pi\Delta f t_k} \end{bmatrix} \cdot \begin{bmatrix} \Delta\hat{\psi} \\ \Delta\mathrm{w} \\ \Delta\mathrm{f} \end{bmatrix}$$

$$= \mathbf{P}(\tilde{\hat{\psi}}) \cdot \mathbf{A} \cdot \tilde{\rho} + \mathbf{P}(\tilde{\hat{\psi}}) \cdot \mathbf{B}(\tilde{\mathrm{w}}, \tilde{\mathrm{f}}) \cdot \begin{bmatrix} \Delta\hat{\psi} \\ \Delta\mathrm{w} \\ \Delta\mathrm{f} \end{bmatrix} \qquad \text{(A.4)}$$

where,

$$\mathbf{B}(\tilde{\mathrm{w}}, \tilde{\mathrm{f}}) = \begin{bmatrix} (\tilde{\mathrm{w}} + \tilde{\mathrm{f}} \cdot e^{j2\pi\Delta f t_1}) \cdot j2\pi t_1 & 1 & e^{j2\pi\Delta f t_1} \\ (\tilde{\mathrm{w}} + \tilde{\mathrm{f}} \cdot e^{j2\pi\Delta f t_2}) \cdot j2\pi t_2 & 1 & e^{j2\pi\Delta f t_2} \\ \cdots & \cdots & \cdots \\ (\tilde{\mathrm{w}} + \tilde{\mathrm{f}} \cdot e^{j2\pi\Delta t_k}) \cdot j2\pi t_k & 1 & e^{j2\pi\Delta t_k} \end{bmatrix}_{kx3}$$

1. Starting from the initial guess of the complex field map $\tilde{\hat{\psi}} = \psi_0$. An initial guess of 0 is used for R2* at all pixels. $\tilde{\hat{\psi}}$ represents the current estimate of the "complex field map."
2. With the estimated $\tilde{\hat{\psi}}$, the corresponding complex water $\tilde{w}$ and fat $\tilde{f}$ can be determined from a least-squares inversion:

$$\tilde{\rho} = \begin{bmatrix} \tilde{w} \\ \tilde{f} \end{bmatrix} = (A^T A)^{-1} A^T \cdot P(-\tilde{\hat{\psi}}) \cdot s \qquad (A.2)$$

   where $\mathbf{A}^T$ represents the complex conjugate transpose of the $\mathbf{A}$ matrix. Here, we have used the fact that $\mathbf{P}(-\hat{\psi}) \cdot \mathbf{P}(\hat{\psi}) = \mathbf{P}(\hat{\psi}) \cdot \mathbf{P}(-\hat{\psi}) = \mathbf{I}$.

3. Equation (1) can be approximated by Taylor expansion as in the following, with the second and higher-order terms neglected.

$$s_i = (\tilde{w} + \tilde{f} \cdot e^{j2\pi\Delta f t_i}) \cdot e^{j2\pi\tilde{\hat{\psi}} t_i} + e^{j2\pi\tilde{\hat{\psi}} t_i} \cdot \Delta w + e^{j2\pi\tilde{\hat{\psi}} t_i} \cdot e^{j2\pi\Delta f t_i} \Delta f + (\tilde{w} + \tilde{f} \cdot e^{j2\pi\Delta f t_i}) \cdot e^{j2\pi\tilde{\hat{\psi}} t_i} \cdot j2\pi t_i \cdot \Delta\hat{\psi} \qquad (A.3)$$

   Considering all echoes, Eq. (A.3) can be formulated in a matrix form:

$$= P(\tilde{\hat{\psi}}) \cdot A \cdot \tilde{\rho} + P(\tilde{\hat{\psi}}) \cdot B(\tilde{w},\tilde{f}) \cdot \begin{bmatrix} \Delta\hat{\psi} \\ \Delta w \\ \Delta f \end{bmatrix} \qquad (A.4)$$

   where,

$$B(\tilde{w},\tilde{f}) = \begin{bmatrix} (\tilde{w} + \tilde{f} \cdot e^{j2\pi\Delta f t_1}) \cdot j2\pi t_1 & 1 & e^{j2\pi\Delta f t_1} \\ (\tilde{w} + \tilde{f} \cdot e^{j2\pi\Delta f t_2}) \cdot j2\pi t_2 & 1 & e^{j2\pi\Delta f t_2} \\ \cdots & \cdots & \cdots \\ (\tilde{w} + \tilde{f} \cdot e^{j2\pi\Delta t_k}) \cdot j2\pi t_k & 1 & e^{j2\pi\Delta t_k} \end{bmatrix}_{kx3}$$

   Therefore, error terms can be obtained by another least-squares inversion:

$$\begin{bmatrix} \Delta\hat{\psi} \\ \Delta w \\ \Delta f \end{bmatrix} = (B^T B)^{-1} B^T \cdot (P(-\tilde{\hat{\psi}}) \cdot s - A \cdot \tilde{\rho}) \qquad (A.5)$$

   where $B(\tilde{w},\tilde{f})$ has been simplified as B.

4. Update the estimated complex field map:

$$\tilde{\hat{\psi}} = \tilde{\hat{\psi}} + \Delta\hat{\psi} \qquad (A.6)$$

5. With the new $\tilde{\hat{\psi}}$, repeat steps 2–4 until the following convergence criterion is achieved or a predefined maximum number of iterations (30) is met:

$$|real\{\Delta\hat{\psi}\}| = |\Delta\psi| < \varepsilon \ and$$

$$|imag\{\Delta\hat{\psi}\} \cdot 2\pi| = |R_2^*| < \varepsilon \qquad (A.7)$$

   where ϵ denotes a small number. In practice, $\epsilon = 1$ can be used.

Fat and water separation techniques : IDEAL technique

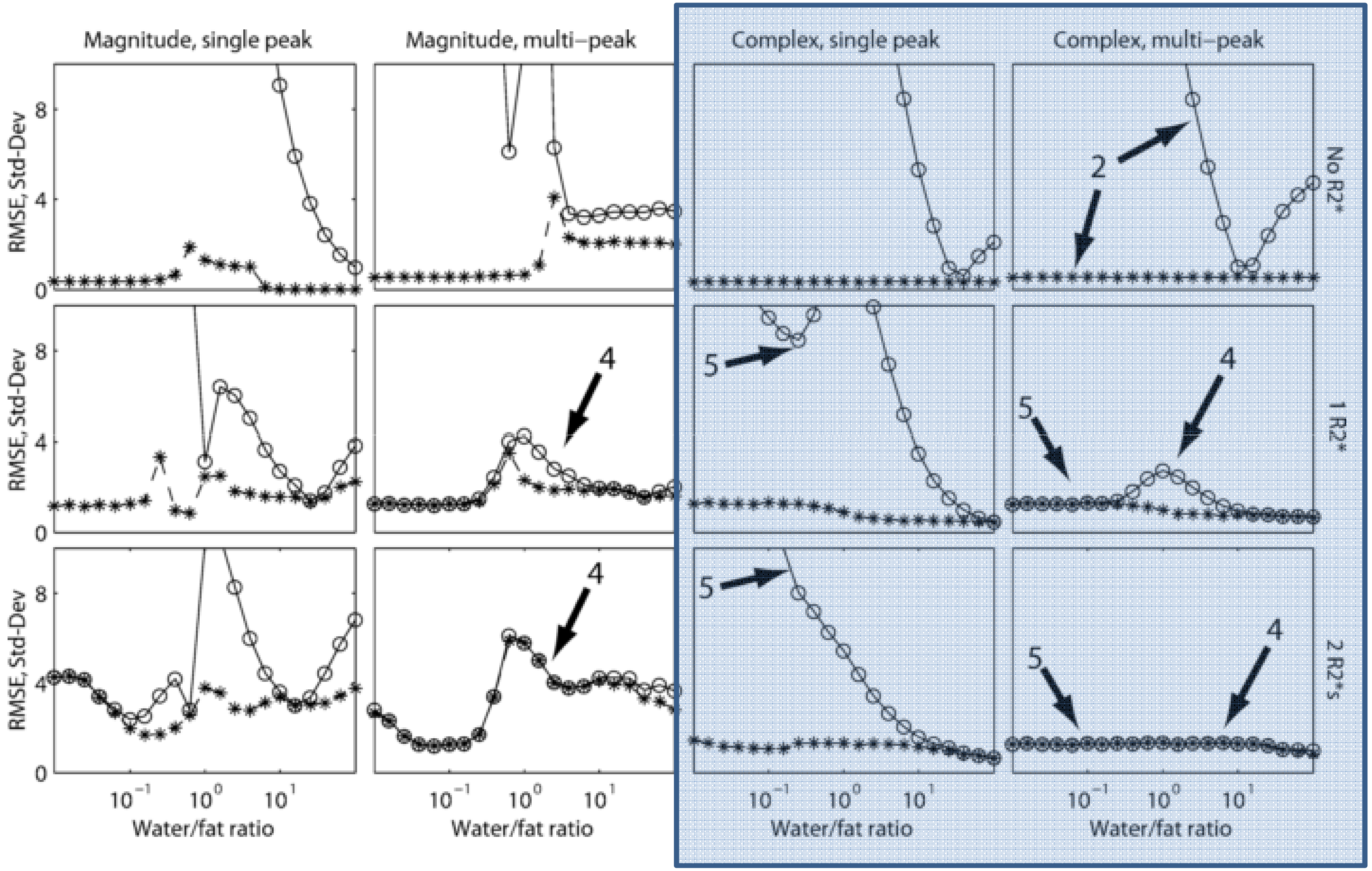

FIG. 4. Fat quantification standard deviation (stars) and RMSE (circles) on simulated data for high SNR (SNR = 100). Arrows with c labels highlight different aspects of these results: "2," in the presence of model mismatch, the bias component of the RMSE significantly larger than the standard deviation; "4," complex fitting generally results in better estimates (lower standard deviati RMSE) compared to magnitude fitting; "5," for one- and two-decay complex fitting, multipeak models largely remove the bias pre single-peak models.

Fat and water separation techniques : IDEAL technique

Iterative reconstruction process : limitations

- IDEAL technique assumes that the initial guess of R2* and B0 field inohomogeniety are close to real values.

- The reconstruction technique can lead to local minimums which can result in false estimation of water and fat signal.

- The algorithm, is a voxel by voxel resolution, no regularization term.

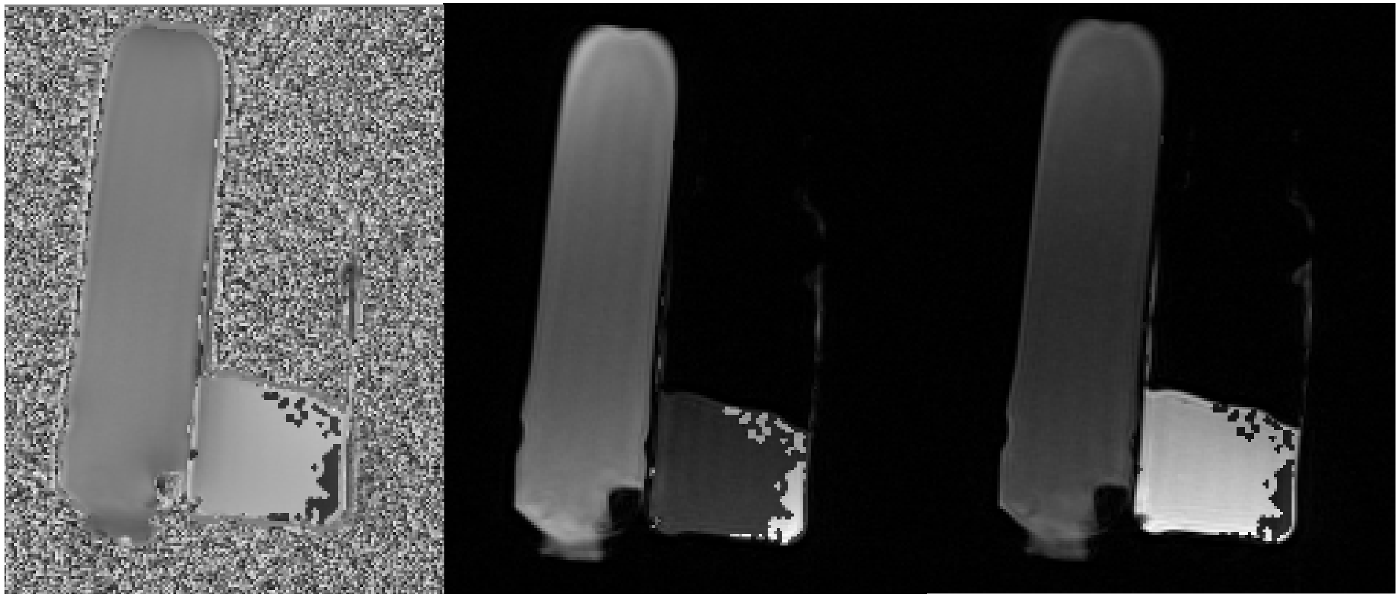

Results of IDEAL technique on mayonnaise samples with different fat ratio : from left to right : field map, water map and fat map.

Magnetic Resonance in Medicine 59:571–580 (2008)

Joint Estimation of Water/Fat Images and Field Inhomogeneity Map

D. Hernando,[1,2]* J. P. Haldar,[1,2] B. P. Sutton,[2,3] J. Ma,[4] P. Kellman,[5] and Z.-P. Liang[1,2]

Global Optimization Using Variable Projection

Estimation of $\{\rho_W, \rho_F, f_B\}$ by minimizing the cost function in Eq. [3] is a separable NLLS problem. Specifically, rewrite Eq. [3] as

$$R_0(\boldsymbol{\rho}, f_B) = \|\mathbf{s} - \boldsymbol{\Psi}(f_B)\boldsymbol{\rho}\|_2^2 \qquad [4]$$

where $\boldsymbol{\rho} = [\rho_W\ \rho_F]^T$, $\mathbf{s} = [s(t_1)\cdots s(t_N)]^T$, and

$$\boldsymbol{\Psi}(f_B) = \begin{pmatrix} e^{i2\pi f_B t_1} & e^{i2\pi(f_F+f_B)t_1} \\ e^{i2\pi f_B t_2} & e^{i2\pi(f_F+f_B)t_2} \\ \vdots & \vdots \\ e^{i2\pi f_B t_N} & e^{i2\pi(f_F+f_B)t_N} \end{pmatrix}. \qquad [5]$$

For a given value of f_B, the least squares (LS) solution for the linear parameters $\boldsymbol{\rho}$ is given by $\boldsymbol{\Psi}^{\dagger}(f_B)\mathbf{s}$, where † denotes pseudoinverse. Therefore, we can remove $\boldsymbol{\rho}$ from Eq. [4]:

$$R(f_B) = \|\mathbf{s} - \boldsymbol{\Psi}(f_B)\boldsymbol{\Psi}^{\dagger}(f_B)\mathbf{s}\|_2^2 = \|[\mathbf{I} - \boldsymbol{\Psi}(f_B)\boldsymbol{\Psi}^{\dagger}(f_B)]\mathbf{s}\|_2^2 \qquad [6]$$

where $\mathbf{I}$ is the $N \times N$ identity matrix. This is the so-called VARPRO formulation of the original NLLS problem in Eq. [4]. It has been shown that $R_0(\boldsymbol{\rho}, f_B)$ and $R(f_B)$ have the same global minimum (7,8). Using Eq. [6], the optimal linear and nonlinear parameters in Eq. [4] can be determined separately as follows

$$f_B^o = \arg\min_{f_B} R(f_B) \qquad [7]$$

$$\boldsymbol{\rho}^o = \boldsymbol{\Psi}^{\dagger}(f_B^o)\mathbf{s}. \qquad [8]$$

The main objective is to address the problem of regularization as well as local minimum problems related to the IDEAL resolution.

Fat and water separation techniques : VARPRO technique

VARPRO: reconstruction amounts to 1D function minimization

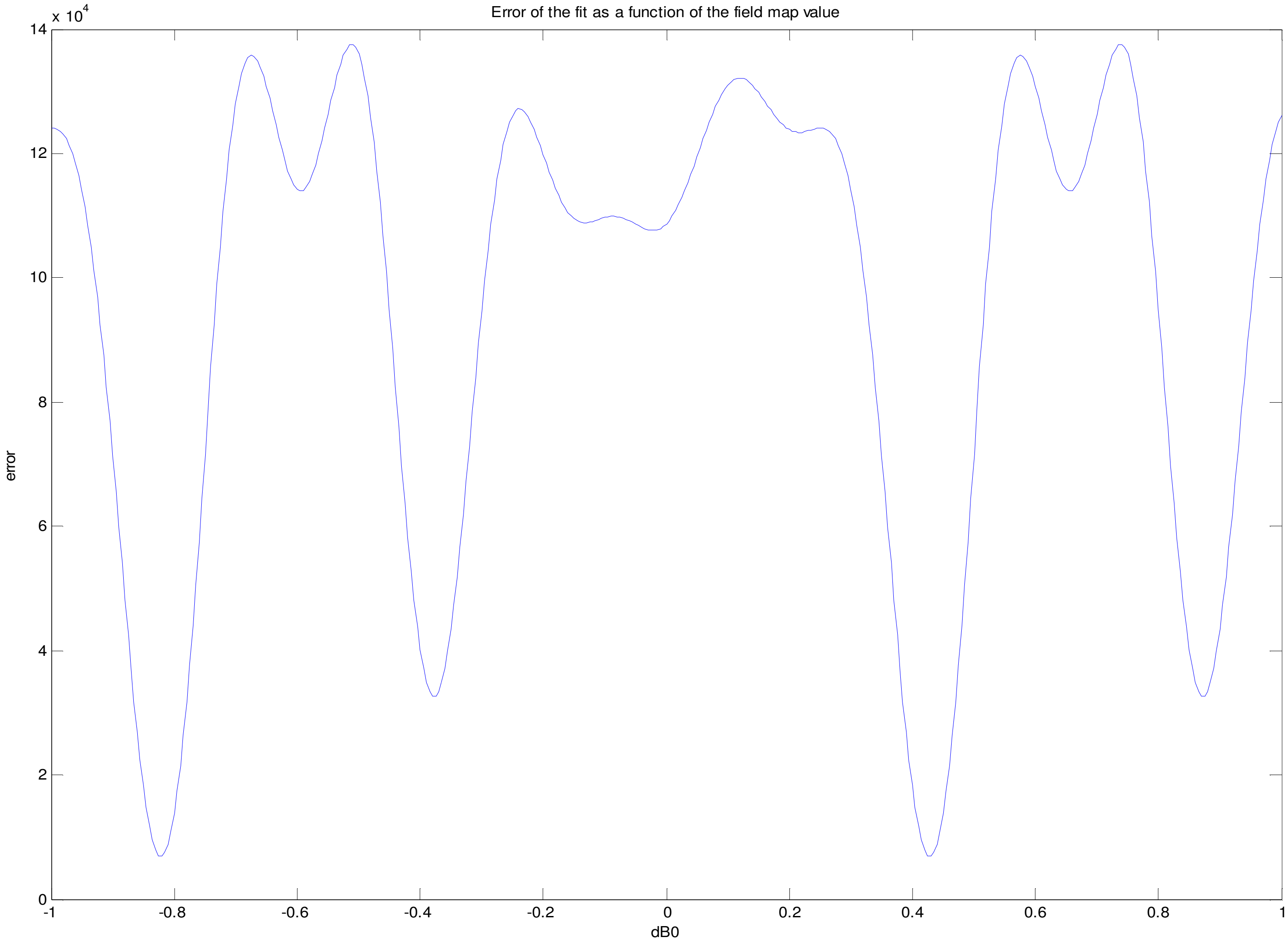

Fat and water separation techniques : VARPRO technique

VARPRO: Algorithm

The VARPRO-based method with MRF prior is summarized below:

1. Initialize the field map estimate $\boldsymbol{f}_{\mathrm{B}}$ (e.g., all zeros).
2. Precompute the cost function $\{R(f_{\mathrm{B},l})\}_{l=1}^{L}$ (Eq. [6]) for a set of field inhomogeneity values $f_{\mathrm{B},l} \in [f_{\mathrm{B,MIN}}, f_{\mathrm{B,MAX}}]$, for all voxels.
3. For each voxel, update the field map estimate using Eq. [10].
4. Repeat step (3) until the overall field map change falls below some small threshold $\varepsilon > 0$:

$$\sum_{q=1}^{Q} \left| f_{\mathrm{B}}^{q,\mathrm{new}} - f_{\mathrm{B}}^{q,\mathrm{cur}} \right| < \varepsilon. \qquad [11]$$

5. For each voxel, estimate ρ_{W} and ρ_{F} given the estimated field map using Eq. [8].

$$f_{\mathrm{B}}^{q,\mathrm{new}} = \arg\min_{f_{\mathrm{B}}^{q}} R(f_{\mathrm{B}}^{q}) + \mu \sum_{j \in \delta_q} w_{q,j} \left| f_{\mathrm{B}}^{q} - f_{\mathrm{B}}^{j,\mathrm{cur}} \right|^2 \qquad [10]$$

where $f_{\mathrm{B}}^{j,\mathrm{cur}}$ is the current field inhomogeneity estimate at neighboring voxel j, $w_{q,j}$ are weights that control the

The algorithm is composed of two main step

1- Minimization

2- Regularization

Fat and water separation techniques : VARPRO technique

VARPRO: comparaison with IDEAL

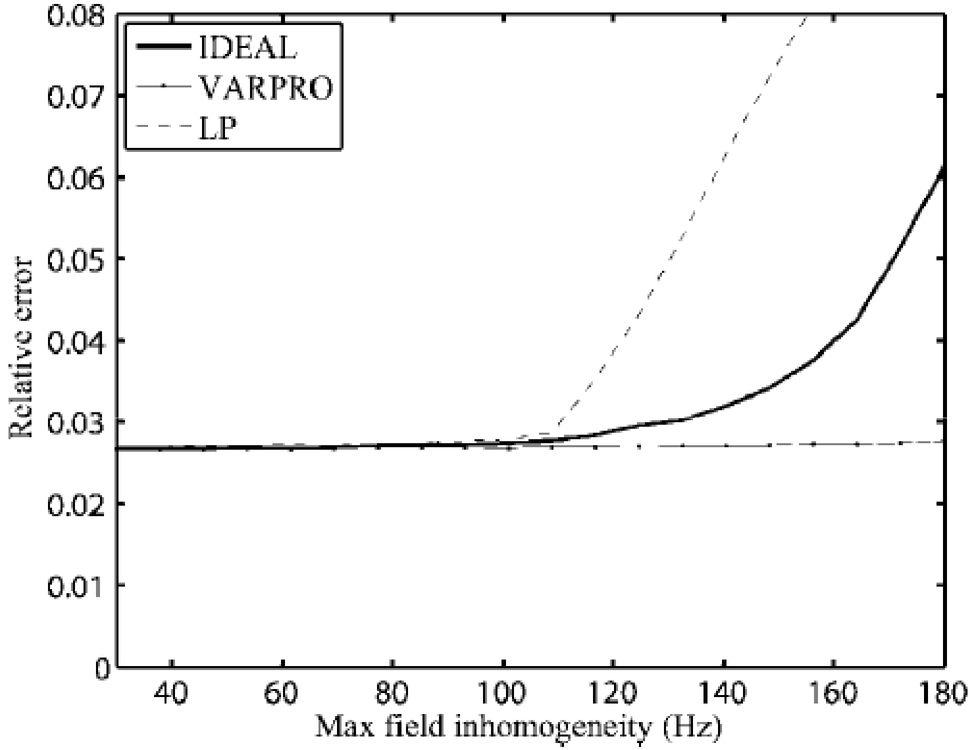

FIG. 2. Quantitative comparison of IDEAL, VARPRO, and LP for water/fat decomposition including spatial smoothness constraints on the field map. Relative errors are shown for water image reconstruction using the three methods, for different levels of field inhomogeneity, and averaged for three different synthetic datasets.

Magnetic Resonance in Medicine 63:79–90 (2010)

Robust Water/Fat Separation in the Presence of Large Field Inhomogeneities Using a Graph Cut Algorithm

Diego Hernando,[1,2*] P. Kellman,[3] J. P. Haldar,[1,2] and Z.-P. Liang[1,2]

An extension of the VARPRO approach, it performs minimization and regularization at the same step

Fat and water separation techniques : VARPRO + Graph cut

3). The signal at an individual voxel q can be described by the simplified model:

$$s_q(t_n) = e^{i2\pi f_{B,q} t_n}(\rho_{W,q} + \rho_{F,q} e^{i2\pi f_F t_n}), \text{ for } n = 1, \ldots, N, \quad [1]$$

Joint Estimation of Water/Fat Images and Field Map

Under the usual assumption of white additive Gaussian noise, the maximum likelihood estimate of $\{\rho_{W,q}, \rho_{F,q}, f_{B,q}\}$ in Eq. [1] is obtained by minimizing the following cost function at each voxel q (as previously proposed (4,16)):

$$R_0(\rho_{W,q}, \rho_{F,q}, f_{B,q}; \mathbf{s}_q) = \sum_{n=1}^{N} \left| s_q(t_n) - e^{i2\pi f_{B,q} t_n}(\rho_{W,q} + \rho_{F,q} e^{i2\pi f_F t_n}) \right|^2 \quad [2]$$

where $\mathbf{s}_q = [s_q(t_1) \cdots s_q(t_N)]^T$.

Dimensionality Reduction Using VARPRO

$R_0(\rho_{W,q}, \rho_{F,q}, f_{B,q}; \mathbf{s}_q)$ has a particular mathematical structure that lends itself straightforwardly to the VARPRO formulation. Specifically, the nonlinear parameter $f_{B,q}$ can be estimated by minimizing (14):

$$R(f_{B,q}; \mathbf{s}_q) = \left\| [\mathbf{I} - \mathbf{\Psi}(f_{B,q}) \mathbf{\Psi}^{\dagger}(f_{B,q})] \mathbf{s}_q \right\|_2^2 \quad [4]$$

where $\mathbf{\Psi}(f_{B,q})$ is a $N \times 2$ matrix with entries $[\mathbf{\Psi}(f_{B,q})]_{(n,1)} = e^{i2\pi f_B t_n}$ and $[\mathbf{\Psi}(f_{B,q})]_{(n,2)} = e^{i2\pi (f_F + f_{B,q}) t_n}$, for $n = 1, \ldots, N$, and † denotes pseudoinverse.

$$\{\hat{\rho}_W, \hat{\rho}_F, \hat{\mathbf{f}}_B\} = \underset{\substack{\mathbf{f}_B \in \mathbb{R}^Q \\ \rho_W, \rho_F \in \mathbb{C}^Q}}{\arg\min} \sum_{q=1}^{Q} R_0(\rho_{W,q}, \rho_{F,q}, f_{B,q}; \mathbf{s}_q) + \mu \sum_{q=1}^{Q} \sum_{j \in \delta_q} w_{q,j} V(f_{B,q}, f_{B,j}) \quad [3]$$

$$\hat{\mathbf{f}}_B = \underset{\mathbf{f}_B \in \mathbb{R}^Q}{\arg\min} \sum_{q=1}^{Q} R(f_{B,q}; \mathbf{s}_q) + \mu \sum_{q=1}^{Q} \sum_{j \in \delta_q} w_{q,j} V(f_{B,q}, f_{B,j}), \quad [5]$$

Discrete optimization technique like graph cut or other approaches

Fat and water separation techniques : VARPRO + Graph cut

FIG. 4. Comparison of the proposed method with two previously proposed methods (ICM and voxel independent). In this dataset, field inhomogeneities near the edges of the FOV are relatively moderate because it was not acquired on a wide-bore scanner. (Top) Field maps. (Center) Water images. (Bottom) Fat images. ICM and voxel-independent methods resulted in water/fat swaps (indicated by arrows) in the liver under the dome of the diaphragm, as well as in the subcutaneous fat, but the proposed method produced good water/fat separation.

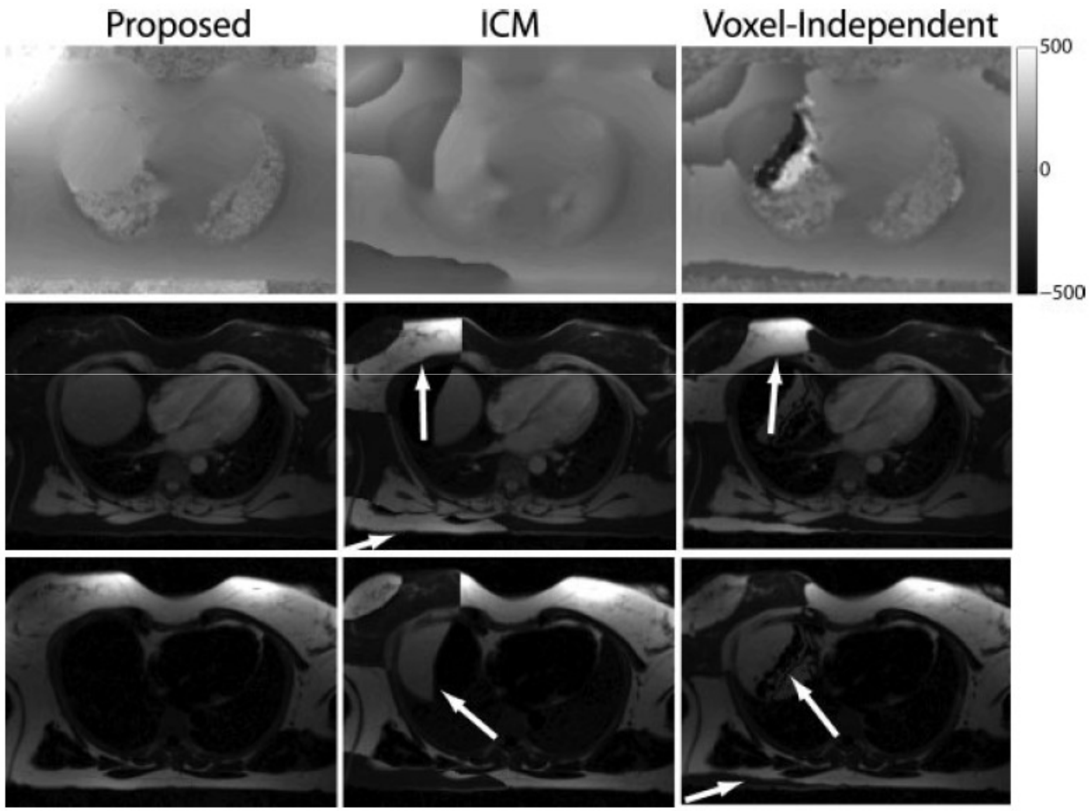

Fat and water separation techniques : Summary

Two element are crucial in the estimation of fat and water signal in the tissue :

1- Accurate signal model : R2* decay and multi-peak fat spectrum
2- Efficient global optimization approach, on complex data.

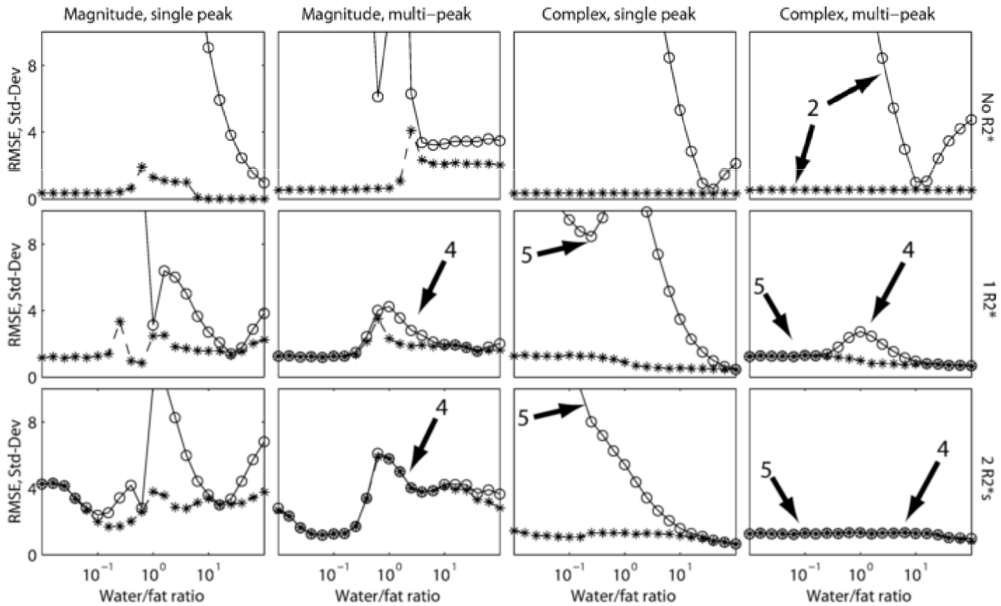

FIG. 4. Fat quantification standard deviation (stars) and RMSE (circles) on simulated data for high SNR (SNR = 100). Arrows with c labels highlight different aspects of these results: "2," in the presence of model mismatch, the bias component of the RMSE significantly larger than the standard deviation; "4," complex fitting generally results in better estimates (lower standard deviati RMSE) compared to magnitude fitting; "5," for one- and two-decay complex fitting, multipeak models largely remove the bias pr single-peak models.

Fat and water separation techniques : IDEAL technique

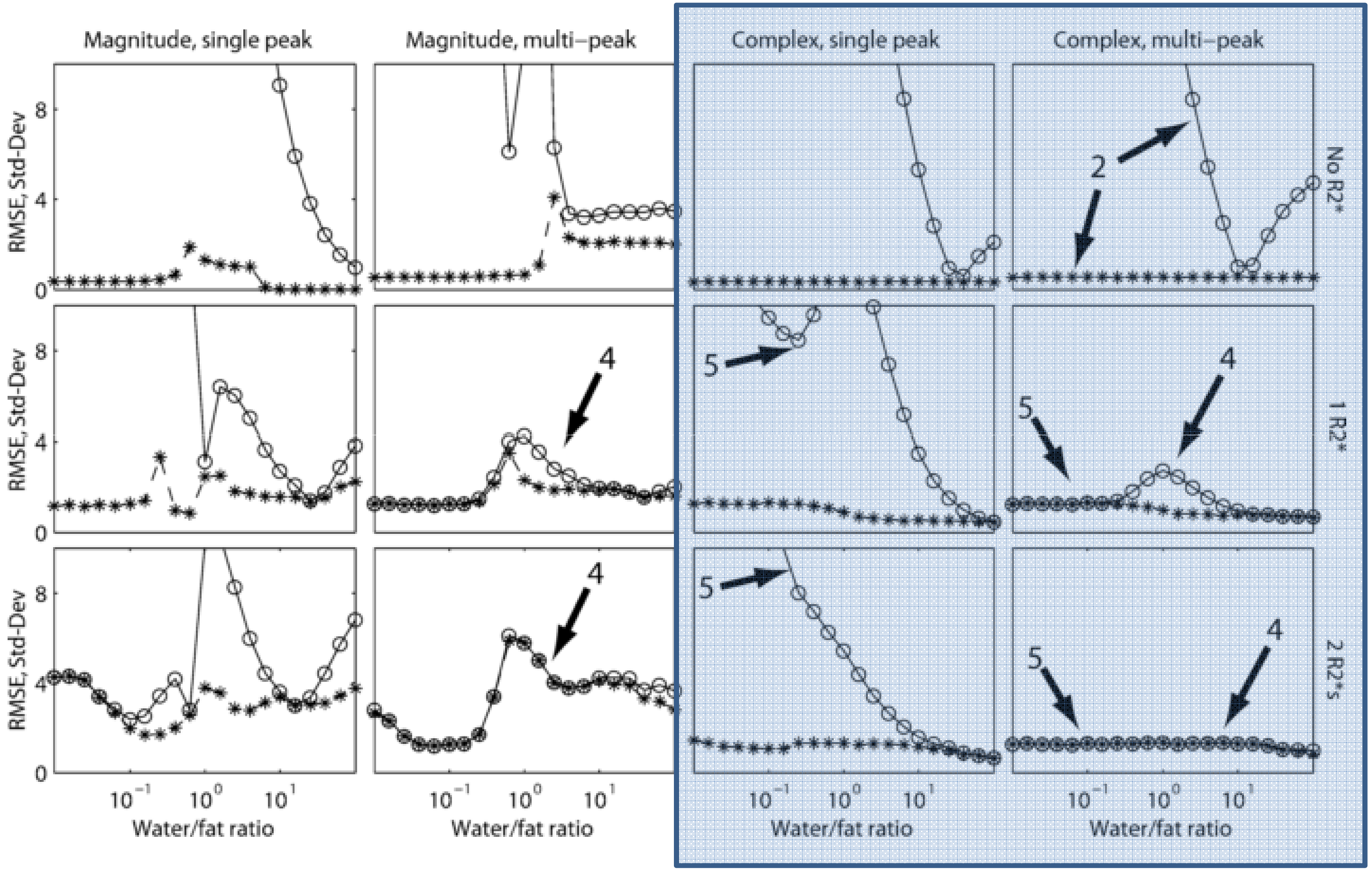

FIG. 4. Fat quantification standard deviation (stars) and RMSE (circles) on simulated data for high SNR (SNR = 100). Arrows with c
labels highlight different aspects of these results: "2," in the presence of model mismatch, the bias component of the RMSE
significantly larger than the standard deviation; "4," complex fitting generally results in better estimates (lower standard deviati
RMSE) compared to magnitude fitting; "5," for one- and two-decay complex fitting, multipeak models largely remove the bias pr
single-peak models.

Fat and water separation techniques : Impact of fat spectrum

Taking into account M peaks, requires the acquisition of M+2 images

➔ Exam duration is increased

Pre-calibration of fat spectrum :

$$s_n = \left(w + \sum_{k=1}^{M} \rho_k \, e^{i2\pi\Delta f_k t_n} \right) e^{i2\pi\psi t_n} e^{-t_n R_2^*}$$

$$\Downarrow$$

$$s_n = \left(w + F \sum_{k=1}^{M} \rho_k \, e^{i2\pi\Delta f_k t_n} \right) e^{i2\pi\psi t_n} e^{-t_n R_2^*}$$

Fat and water separation techniques : Impact of fat spectrum

$$s_n = \left(w + \sum_{k=1}^{M} \rho_k \, e^{i2\pi\Delta f_k t_n} \right) e^{i2\pi\psi t_n} e^{-t_n R_2^*} \qquad s_n = \left(w + F \sum_{k=1}^{M} \rho_k \, e^{i2\pi\Delta f_k t_n} \right) e^{i2\pi\psi t_n} e^{-t_n R_2^*}$$

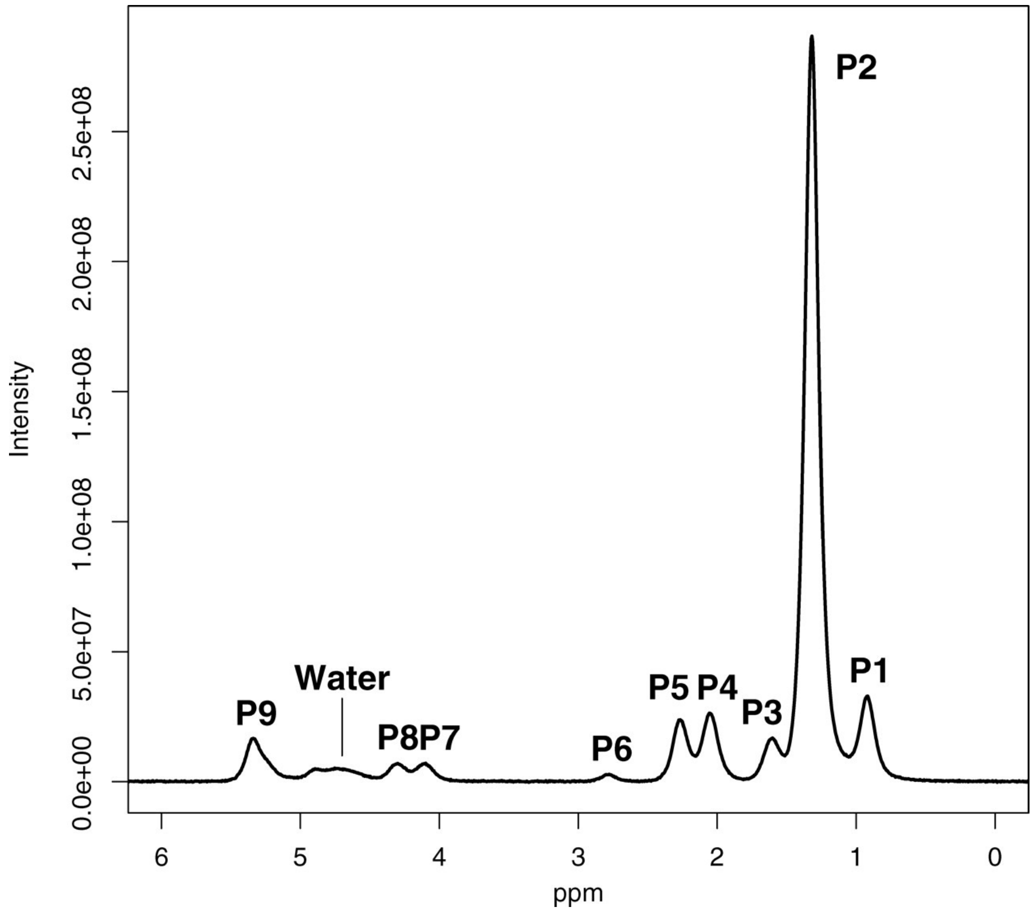

Fat and water separation techniques : Impact of fat spectrum

$$s_n = \left(w + \sum_{k=1}^{M} \rho_k \, e^{i2\pi\Delta f_k t_n} \right) e^{i2\pi\psi t_n} e^{-t_n R_2^*} \qquad s_n = \left(w + F \sum_{k=1}^{M} \rho_k \, e^{i2\pi\Delta f_k t_n} \right) e^{i2\pi\psi t_n} e^{-t_n R_2^*}$$

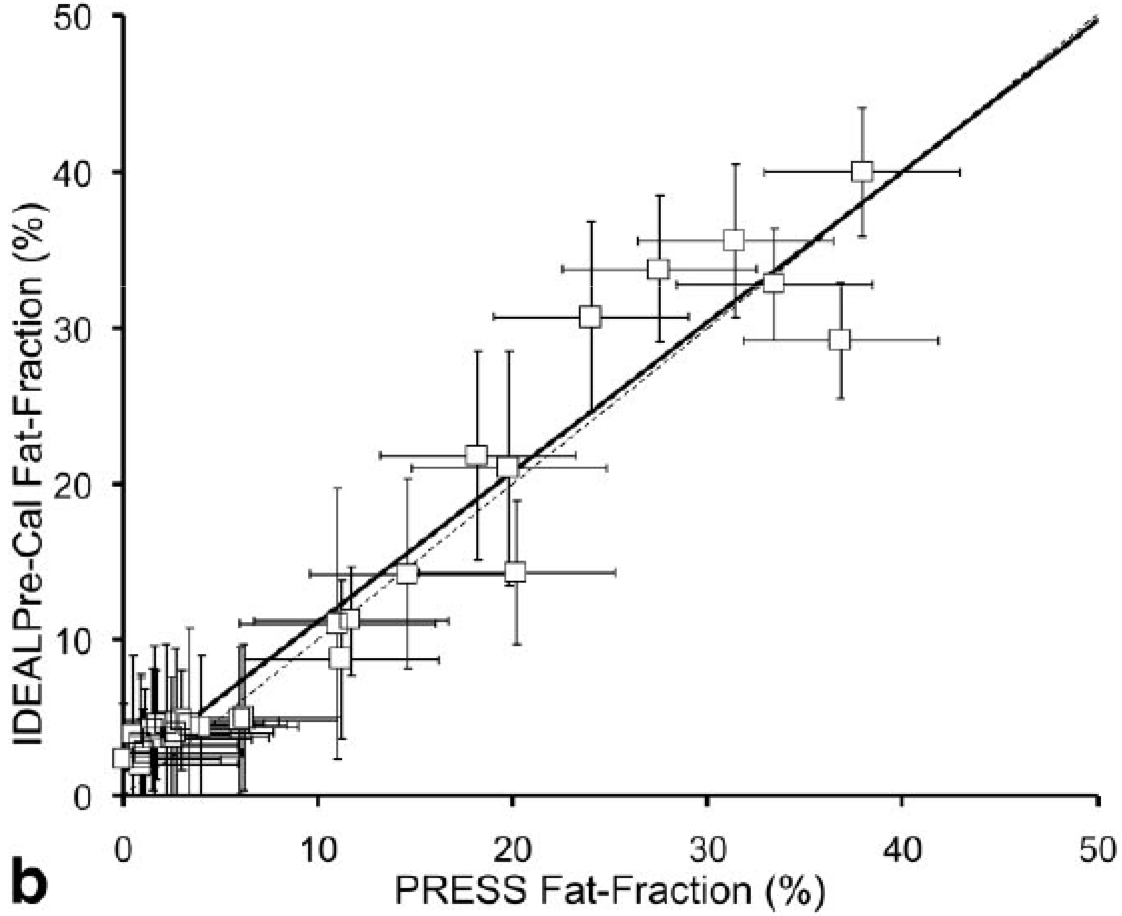

Fat and water separation techniques : Echo time selection

The Cramér–Rao Bound

At the heart of the CRB is the Fisher information matrix (FIM) (9, 10). It can be interpreted as the sensitivity of the data to the parameters being estimated taking into account the noise,

$$F_{kl} = -\left\langle \frac{\partial}{\partial p_k} \frac{\partial}{\partial p_l} \ln Pr(\mathbf{s}|\mathbf{p}) \right\rangle, \qquad [2]$$

where $\mathbf{s}$ is the vector containing the data, $\mathbf{p}$ is the vector containing the parameters of the model and $Pr(\mathbf{s}|\mathbf{p})$ is the probability of observing $\mathbf{s}$ given $\mathbf{p}$.

The variance of the estimator verifies $\sigma^2_{\hat{p}_k} \geq [F^{-1}]_{kk}$.

Three-Point Technique of Fat Quantification of Muscle Tissue as a Marker of Disease Progression in Duchenne Muscular Dystrophy: Preliminary Study

Tishya A. L. Wren[1]
Stefan Bluml
Linda Tseng-Ong
Vicente Gilsanz

[1]All authors: Department of Radiology, Children's Hospital Los Angeles, 4650 Sunset Blvd., MS#81, Los Angeles, CA 90027. Address correspondence to V. Gilsanz (vgilsanz@chla.usc.edu).

AJR:190, January 2008

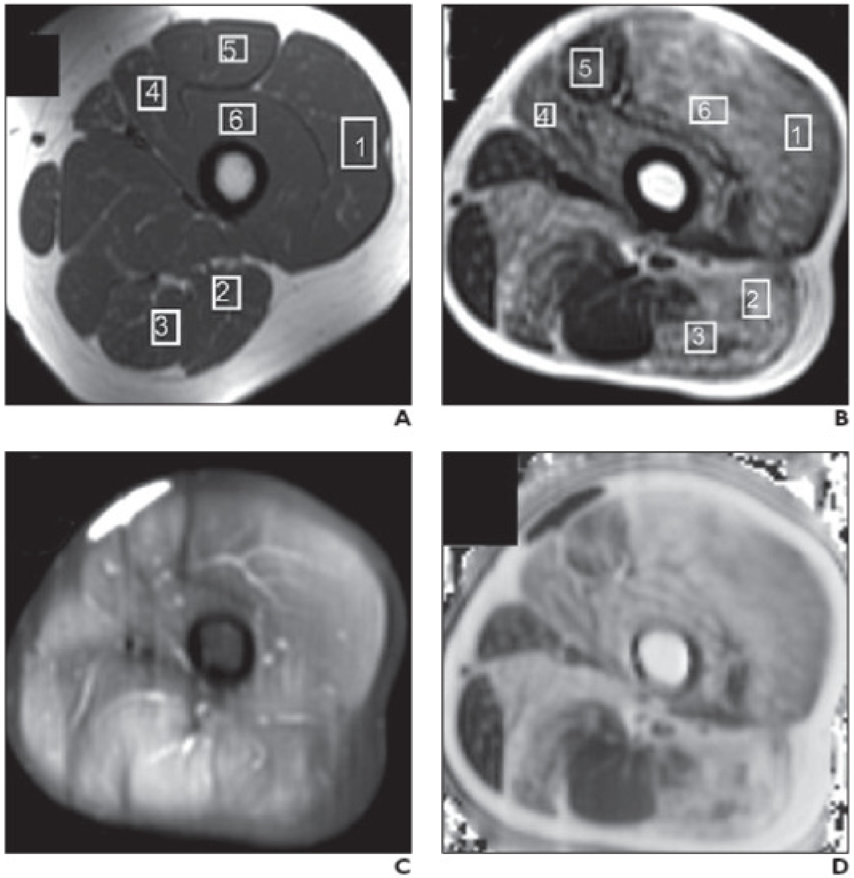

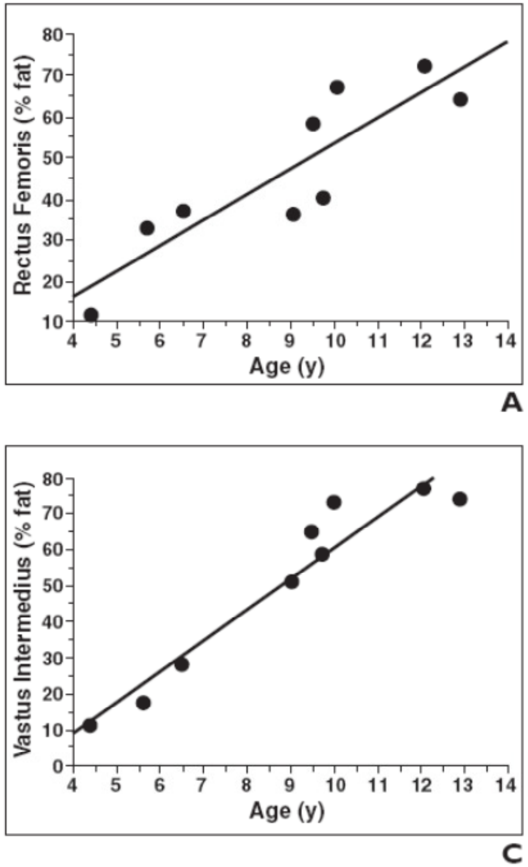

OBJECTIVE. Clinical trials involving patients with Duchenne muscular dystrophy are hindered by the lack of suitable objective end points. The purpose of this study was to examine whether muscle lipid infiltration measured with the three-point Dixon MRI technique has value as a marker of disease severity.

SUBJECTS AND METHODS. Disease severity in nine boys (mean age, 8.6 ± 2.7 years) with Duchenne muscular dystrophy was determined with the functional ability scale of Brooke and associates. Functional scores were compared with strength measurements obtained by manual testing of muscles of the lower extremities, knee extensor strength measured with an isokinetic dynamometer, and muscle fat percentage in the quadriceps and hamstrings determined with the three-point Dixon MRI technique.

RESULTS. MRI measurements of fat infiltration had stronger correlation ($p < 0.05$) with functional grade than did measurements obtained with manual muscle testing ($p = 0.07$) or quantitative strength measured with the isokinetic dynamometer ($p = 0.54$). Muscle fat percentage did not correlate with strength measurements from manual or dynamometer muscle testing but increased with age in subjects with Duchenne muscular dystrophy.

CONCLUSION. Muscle adiposity values obtained with three-point Dixon MRI are accurate in assessment of disease severity in patients with Duchenne muscular dystrophy. Because they are not influenced by patient effort or examiner variability, these measurements are more objective and reproducible than measurements of muscle strength.

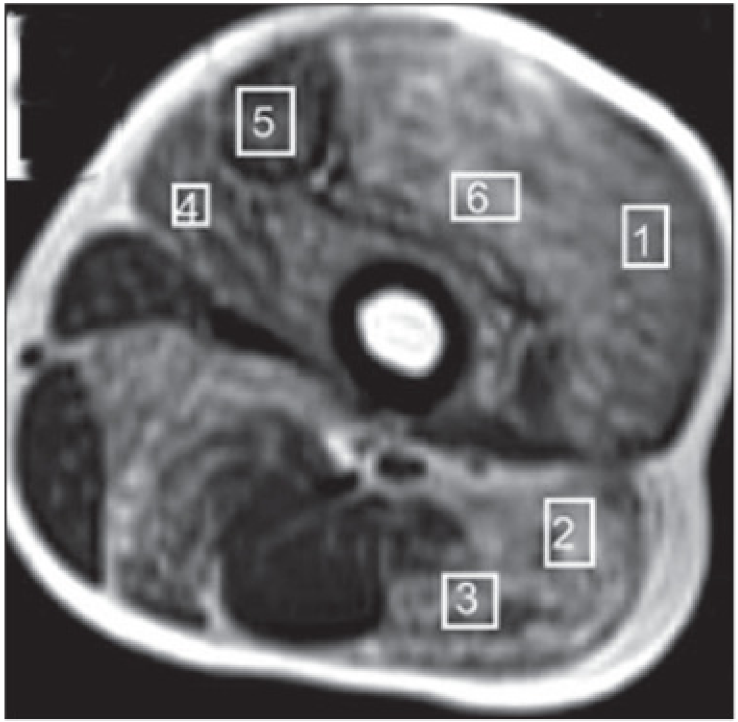

T1-weighted spin-echo MR images (TR/TE, 400/10) obtained in 10-year-old patient with functional score of 3.

1 = vastus lateralis, 2 = biceps femoris, 3 = semitendinosus, 4 = vastus medialis, 5 = rectus femoris, 6 = vastus intermedius.

TABLE 1: Functional Grades According to Scale of Brooke and Associates

Grade	Function
1	Walks and climbs stairs without assistance
2	Walks and climbs stairs with aid of railing
3	Walks and climbs stairs slowly with aid of railing (12 s for four standard stairs)
4	Walks unassisted and rises from chair but cannot climb stairs
5	Walks unassisted but cannot rise from chair or climb stairs
6	Walks only with assistance or walks independently with long leg braces
7	Walks in long leg braces but needs assistance for balance
8	Stands in long leg braces but unable to walk even with assistance

Functional grade was strongly inversely correlated with fat percentage measured with the Dixon technique ($p < 0.05$)

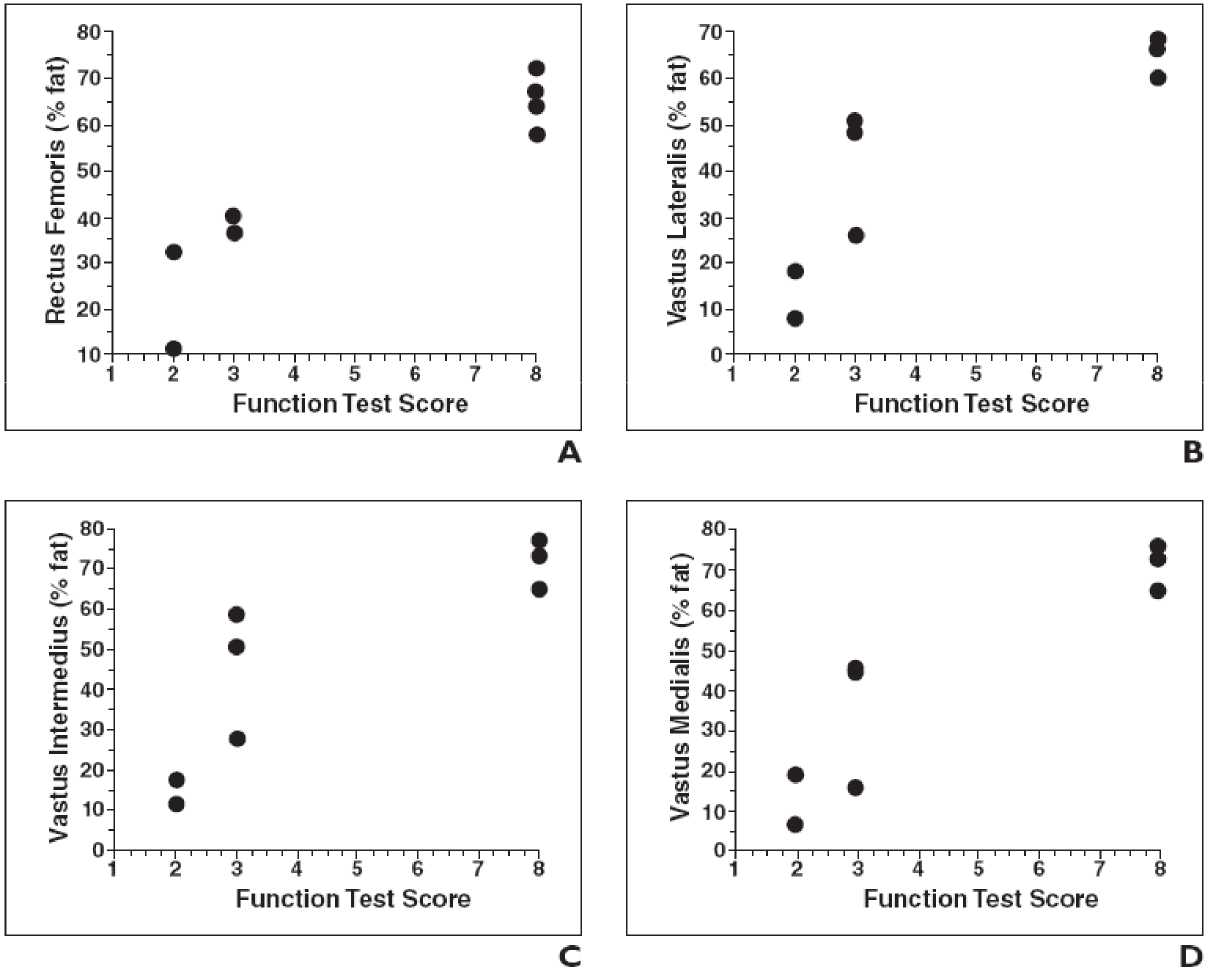

Fig. 3—Graphs show Dixon MRI measurements of intramuscular fat percentage increased significantly with decreasing functional level in all muscles examined.